بِسْمِ اللَّهِ الرَّحْمَنِ الرَّحِيمِ

Sudan University for Science and Technology

College of Petroleum Engineering and Technology

Department of Petroleum Exploration Engineering

Theses title:

Integrated Interpretation of Remote Sensing and Satellite Gravity Data - Red Sea Sudan

تفسير متكامل لبيانات الإستشعار عن بعد وبيانات الجاذبية المقاسة بواسطة الأقمار الإصطناعية – البحر الأحمر - السودان

Prepared by:

Esam Eldeen Abdallah

Almeghdad Abd Alrazig

Ahmed Elzubeir Elsayed

Ahmed Mohamed Elfatih

Ahmed Adil

A dissertation submitted to the department of Exploration in partial fulfillment of the requirement for the Bachelor of Science degree in Petroleum Exploration Engineering

Supervisor:

Mr. Mohamed Salah

Oct. 2016

الإستهلال

قال تعالى:

بِسْمِ اللهِ الرَّحْمنِ الرَّحِيمِ

(يَعْلَمُ مَا بَيْنَ أَيْدِيهِمْ وَمَا خَلْفَهُمْ وَلَا يُحِيطُونَ بِهِ عِلْمًا)

سورة طه

Dedication

This accomplishment is dedicated to

Our Parents …

Our brothers and sisters …

Our friends …

Everyone stood with us …

Acknowledgments

In the beginning, we would like to thank Allah for his grace and blessings on us to achieve this work successfully. Also we would like to thank the consortium of Sudan University for Science and Technology, and specially family of petroleum engineering and technology, without excluding anyone from teachers, assistant teachers, colleagues, to personnel of university's libraries.

A special gratitude to our supervisor, Mr. Mohamed Salah, which has guided us with his wise lead and continuous efforts from the inception of this research until it reached its final form. Also we would like to thank Mr. Osman Malik for his cooperation with us which meant a lot to us.

Abstract

The study area lies in NE Sudan and is situated in the Red Sea State It is bounded by latitudes (20° 19' 35.1" _ 21° 34' 20.5" N) and longitudes (36° 53' 37.92" _ 37° 12' 47" E). It cover approximately 3539 sq. km, almost the whole area covered by Mohammed Qol and Dungunab (1:250.000) toposheets of the Sudan Survey Department.

Different digital image processing techniques have been applied to Landsat OLI image in order to increase the discrimination between various lithological units. Image sharpening was performed to enhance the spatial resolution of the image for more detailed information. Contrast stretching was applied, after the various digital processing procedures to produce more interpretable images. The Principal Component Analysis (PCA) transformation yield saturated images and resulted in more interpretable image than the original data. Several ratio images were prepared, combined together and displayed in RGB color composite ratios images.

All the images, obtained through the above mentioned processes, have used simultaneously to produce the geological map of the study area in the GIS environment.

Gravity point data obtained by satellite was used in the present study. Polynomial fitting was used in order to separate the regional from the residual component of the gravity. The first and second vertical derivatives and the first horizontal derivative were computed in order to study the presence of faults. Moreover, two profiles were constructed across the residual gravity map in an approximately NS and NW-SE directions cutting the most prominent anomalies in the area.

The outcome of the present study is the modeling of the subsurface geology of the study area based on the residual gravity map and the above-mentioned two profiles.

التجريد

تقع منطقة الدراسة في شمال شرق السودان وهي تتبع لولاية البحر الأحمر بين خطي عرض ("20.5 '34 °21 _ "35.1 '19 °20) شمالا و خطي طول ("47 '12 °37 _ "37.92 '53 °36) شرقا وهي تغطي مساحة 3539.9 كلم مربع.

أجريت العديد من المعالجات الرقمية لصور الأقمار الصناعية Landsat8 OLI images بغرض زيادة القدرة البصرية على التفريق بين السحنات الصخرية المختلفة. تقنية تحليل المركبات الأساسية قد أنتجت صور بها معلومات أكثر من الصورة الأصلية. وتم إجراء العديد من صور الحزم الطيفية في نظام الألوان (الأحمر, الأخضر و الأزرق). كل العمليات المذكورة أعلاه ساعدت في رسم خريطة جيولوجية لمنطقة الدراسة.

معلومات الجاذبية المستخدمة تم الحصول عليها من القمر الصناعي الامريكي التابع لمعهد المحيطات بجامعة كاليفورنيا. طريقة مطابقة الحدود Polynomial Fitting استخدمت لفصل الجاذبية الإقليمية Regional Gravity عن الجاذبية المتبقية Residual Gravity, تم عمل ثلاثة قطاعات مختلفة على مناطق الشذوذ الموجوده في منطقة الدراسة بإتجاهات شمال جنوب وشمال غرب – جنوب شرق. وأيضاً استخدمت المشتقة الرأسية الأولى و الثانية First and Second Vertical Derivative , وكذلك المشتقة الأفقية الأولى First Horizontal Derivative للتعرف على الفوالق بالمنطقة. و مخرجات هذه الدراسة كانت عبارة عن عمل نموذجين و تحديد سمك الرسوبيات الموجودة فوق صخور الأساس.

LIST OF CONTENTS

CHAPTER ONE: INTRODUCTION

LIST OF FIGURES

LIST OF TABLES

LIST OF PLATES

Chapter One

Introduction

1.1. Location and accessibility:

The study area lies in NE Sudan and is situated in the Red Sea State. It is bounded by latitudes (20° 19' 35.1" _ 21° 34' 20.5" N) and longitudes (36° 53' 37.92" _ 37° 12' 47" E). It covers approximately 3539 sq. km. almost the whole area covered by Mohammed Qol and Dunghunab (1:250.000) topo sheets of the Sudan Survey Department.

The study area is accessible through Port Sudan city (approximately 900 km away from Khartoum).

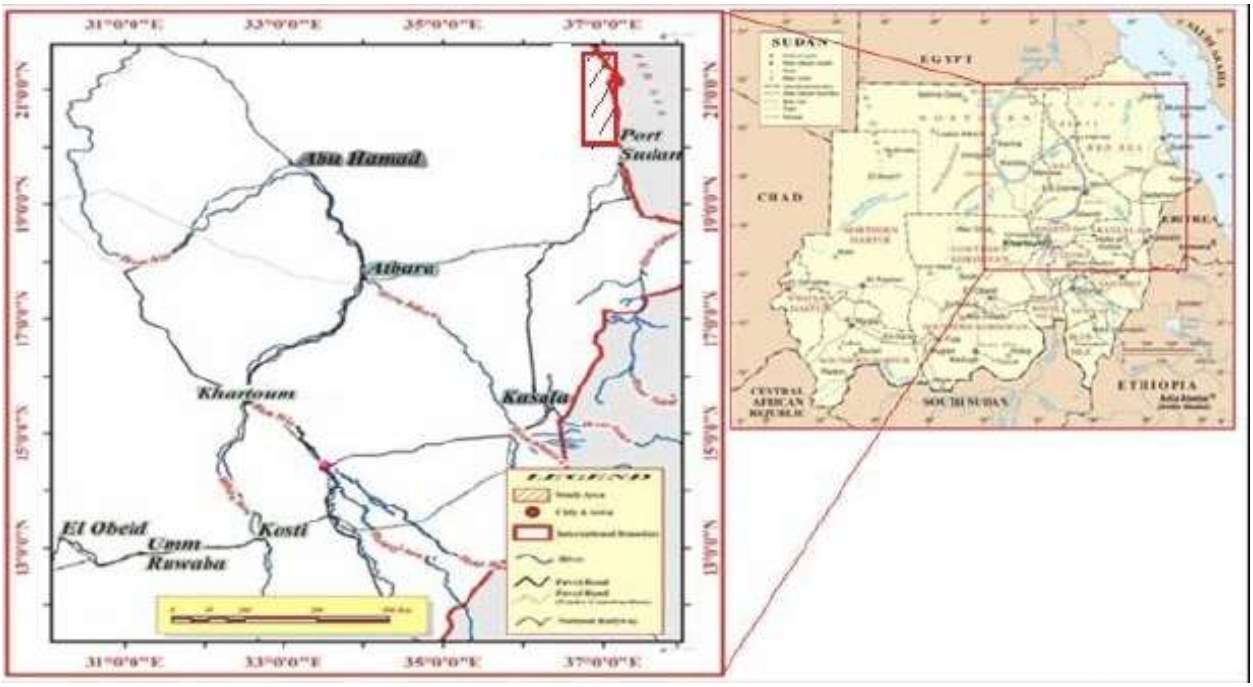

Fig (1.1.): Map shows the location, of study area**.**

1.2. **Topography:**

Geomorphologically, the study area represents part of the high rugged Red Sea Hills terrain, sloping rapidly to the east towards the Red Sea relatively and gently to the west towards the Nile. Jebel Erba represents the highest peak (2150m) in the Red Sea area. This high terrain is an integral part of the upper Eocene uplift of the African-Arabian swell (MOHR, 1971). This swell was later divided by the East African Rift system into an eastern Arabian and a western Nubian part.

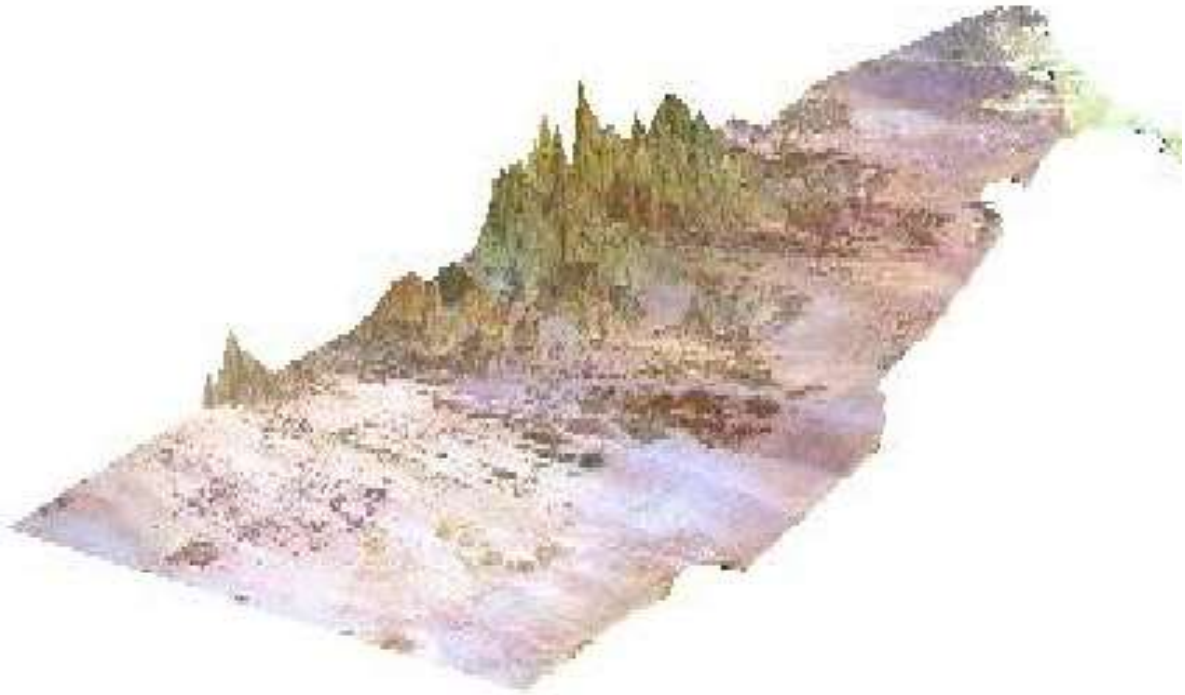

Fig (1.2.): Showing the variation of topography in study area.

1.3. **Climate:**

The Red Sea coastline lies at the edge of two global weather systems that fluctuate seasonally, with changes in prevailing winds, rainfall, water circulation patterns, and air temperatures. The arid nature of the region, hot climate, high levels of solar radiation, limited rainfall, absence of rivers, and seasonal variability in wind direction together create some of the harshest environmental conditions found in the tropics.

1.4. Drainage:

The Red Sea Hills terrain is intensively dissected by a complex drainage network. The dominating drainage systems are highly controlled by the prevailing structural elements of the region. Other physiographic features of the area include the coastal strip and the Red Sea. The drainage system in the northern portion of the Coastal Plain consists of numerous seasonal streams (Wadies and Khors) such as Khor Arbaat, Khor Eit and Khor Shinab, which flow only in seasons of heavy rains.

1.5. Objectives of the study:

The main objective of this study is to carry out more detail Geological-Geophysical investigation in the area North of Port Sudan and its offshore continuation making use of the available data (gravity data and surface geological investigations) and to reveal the subsurface structural elements of the area and to produce 2.5D gravity model in the area.

1.6. Previous studies:

The study area has been the object of several works which covered a wide range of topics including general geology, economic geology, applied geophysics and tectonics.

- **Agip Mineraria (1959-1962)**

Worked on the general geology in the Red Sea by conducting detailed geological and geophysical work in the Sudanese Coast, which led to the drilling of six boreholes.

- **Swartz (1960)**

Described the geological history of the Red Sea.

- **The department of Mineral Resources of Sudan and The Soviet Technical Aid Program (1976)**

Have done a regional geological mapping and prospecting activities in the area.

- **Carella and Scarpa (1962)**

Worked on the stratigraphy of the Sudanese Red Sea Coastal area.

- **Sestini (1965)**

Tried to correlate the stratigraphy of the Red Sea with that of the Gulf of Suez.

- **Bunter and A.Magid (1989)**

Revised the stratigraphy of the Sudanese Red Sea and suggested a new nomenclature in accordance with the nomenclature of the Gulf of Suez.

- **Phillips et al. (1969)**

Studied magnetic and gravity anomalies in the Central Red Sea.

- **Qureshi (1971)**

Conducted gravity survey on the shore of the study area.

- **Saudi-Sudanese Red Sea joint Commission (1975)**

They conducted comprehensive geophysical, oceanographic and environmental surveys.

- **Searle and Rose (1975)**

Conducted ship-borne gravity measurements which resulted in the construction of a 1:1000000 scale Bouguer anomaly map.

- **Chevron Oil Company (1975)**

Produced 1:250000 scale Bouguer anomaly map, a seismic survey and drilled three boreholes in the southern part of the Sudanese Red Sea.

- **Union Texas (1980)**

Recorded 990 km of seismic data in Suakin-Bashayer area.

- **Ezzeldin (1987)**

Studied the tectonics of the Red Sea by interpreting and compiling seismic, gravity and magnetic surveys in the central part of the Red Sea and investigated the structures and the evolution of the Red Sea.

- **Sadig et al. (1987):**

Completed gravity and magnetic traverse from PortSudan to Abu Hamad.

- **Makris and Henke (1992)**

Published a paper on Pull-Apart evolution of the Red Sea.

- **Robertson Research International R.R.I (1988)**

Studied the petroleum geology of the Red Sea by evaluating available data of the petroleum potential of the Sudanese Red Sea.

- **Beydoun (1989)**

Presented a study submitted by the United Nations Development Program, which revealed the presence of Miocene reservoirs and source rocks in the study area.

1.7. **Problem Statement:**

The Study area has been investigated by several major oilfield companies such as Chevron and Total. Those companies employed geophysical methods including conventional potential fields. The outcomes of these surveys revealed the importance and promising prospects of Sudanese Red Sea region, hence a much more sophisticated technologies were needed for the sake of a better imaging and mapping of the surface and subsurface of the area. The technology which we adopted in this research satisfies this needs as we utilize affordable & latest satellites data, and advanced software as means of data processing and interpretation.

Chapter two

Regional Geology & Tectonic Setting

2.1. Introduction:

Formation of the Red Sea and its surrounding features is the result of many interrelated events. The fact that Red Sea structures are now an integral part of the world plate-tectonic system has obscured its earlier geologic development. Time of origin is obscure, but all evidence points toward the early Tertiary.

The first major stratigraphic unit includes all igneous and metamorphic rocks of the "Basement Complex," which forms the Red Sea Hills and the foothills, and is generally considered to be of Precambrian age. In the basement complex," Ruxton (1956) distinguished one metamorphic and two sedimentary and volcanic groups, separated by important unconformities, and affected by various kinds of intrusions. A large granitic batholith trending north-south is exposed in the mountains west of the area of this study.

A late Cretaceous to Cenozoic sequence of variable thickness lies unconformably over the "Basement Complex." The Cretaceous beds occur only in the subsurface at Mukawar Island (Mukawar Formation). The Cenozoic outcrop includes a middle Miocene clastic-carbonate series in the lower part, and a clastic post-middle Miocene series in the upper part.

2.2. Formations sequence:

A Late Cretaceous to Cenozoic sequence of variable thickness lies unconformably over the "Basement Complex." The Cretaceous beds occur only in the subsurface at Mukawar Island (Mukawar Formation). The Cenozoic outcrop includes a middle Miocene clastic-carbonate series in the lower part, and a clastic post-middle Miocene series in the upper part.

2.2.1. **Pre-middle Miocene formations:**

2.2.1.1. **Mukawar Formation**

Formations underlying the middle Miocene part of the sequence were found only in the Mukawar Island-Dongunab region. The Mukawar Formation (90 meters thick) was named by Carella and Scarpa (1962) for beds penetrated in a well drilled in the northern part of Mukawar Island. They are chiefly dark gray silty shales interbedded with fine to medium red and gray sandstones.

2.2.1.2. **Hamamit Formation**

The Hamamit Formation crops out at Jebel Hamamit north of Dongunab (Fig. 2.2.1), and in low hills near the crystalline foothills, west of Dongunab Bay. Beds related to this formation also were found in a boring at Mukawar Island. At Jebel Hamamit, a 30-m.-thick basaltic layer occurs in the middle part of this unit. The formation ranges in thickness from 226 to 266 m. Information on the boundaries is scanty, especially the lower one.

Available evidence suggests a possibly unconformable contact with the underlying Mukawar Formation and a conformable contact with the overlying Maghersum Formation.

2.2.2. **Middle Miocene Series:**

2.2.2.1. **Maghersum Formation**

This name was given by Carella and Scarpa (1962) to a sandstone sequence which crops out on the island of Mukawar. Thin-bedded, medium- to fine-grained calcareous sands predominate at Khor Eit and in the northern part of Jebel Tobanam. In some intervals the sands are interbedded with red, silty, and sandy clays, and north of Khor el Kuk. The matrix is coarse pebbly sand and there is no clay. The sands of the Maghersum Formation are poorly sorted and poorly rounded. There is a variable quantity of colored minerals, such as biotite, magnetite, hornblende, garnet, and limonite. Some fine grained metamorphics and granite have contributed to the sediments, especially in the Jebel Saghum area. The carbonate zones of the Maghersum Formation increase in number from south to north. The measured thickness of the Maghersum Formation is 165 meters at Khor Eit, 95 meters at Khor el Kuk, and 30 meters in the western part of Jebel Saghum. No macro- or microfossils were found in the elastics of the formation in the area studied, but the reefs of the Khor el Kuk section indicate a middle Miocene age (D'Arch. Edw. & H.).

2.2.2.2. **Khor Eit Formation**

The name Khor Eit Formation is proposed for a unit with transitional characters of mixed carbonates and elastics, intervening between the lower clastic and the upper carbonate parts of the Miocene series. The thickness of the formation is 51 m. at Khor Eit and 90 m. at Jebel Tobanam.

The lower two-thirds of the Khor Eit Formation are characterized by the alternation of sand and gravel, with argillaceous and sandy to cobbly limestones .The grain size of most of the clastic zones decreases progressively upward, from fine gravel, through medium to fine sand. The coarser elements are 7-12-cm. cobbles. The color and mineral composition of the sand and gravel of the Khor Eit Formation are the same as in the Maghersum Formation.

The upper third of the Khor Eit Formation is more calcareous and it displays considerable lateral lithological variations. Some units locally are very fossiliferous. At Khor Eit, an interval of sandy, soft white limestone contains small coral colonies.

2.2.2.3. **Abu Imama Formation**

The Abu Imama Formation was named by Carella and Scarpa (1962) from an exposure of reef limestones at Jebel Abu Imama, north of Muhammed Qol. In the area studied by the writer, this formation constitutes the main part of the Eit Jebel and most of the homoclinal hills of the eastern part of Jebel Tobanam. It exhibits the least amount of lateral variation and has a constant measured thickness of 45 meters. The macro- and microfossils in the Abu Imama limestones of the area studied are indicative of early to middle Miocene age, with a preference for the middle Miocene.

2.2.3. **Post-Middle Miocene Series:**

2.2.3.1. **Dongunab Formation**

In the area east of Eit Well, a formation composed chiefly of sands and correlating with the Dongunab Formation of Carella and Scarpa (1962) crops out not much above the uppermost Abu Imama limestones. The contact between the two units is covered, but the dip and strike of the beds are not suggestive of an unconformity. The exposure is 32 m. thick and includes medium to coarse, white sands, commonly pebbly, brown or red sandy and silty clays, thin lenses of pebble-gravel and a few beds of gypsum up to 10 cm. thick. The carbonate content is very limited. The age of these sediments in the Eit area cannot be determined because no fossils were found. In the Dongunab region, the formation is 722 m. thick. It rests unconformably on the Abu Imama limestones and includes a thick interval of gypsum and salt. This unit possibly correlates with the late Miocene Evaporite Formation of the Egyptian sequence (Gulf of Suez and Quseir).

2.2.3.2. **Upper Clastic Group**

The Abu Imama and Dongunab formations both are overlain unconformably by a clastic sequence composed chiefly of coarse gravel with sand lenses. The clastic complex crops out extensively in the area, mostly underlying the recent sands of the plain, but also occurs as terraces at two higher levels. The upper boundary, as seen in outcrops, is an unconformable contact with the emergent reefs of the coast (Berry and Sestini, in preparation). The stratigraphy of the complex was not worked out in detail, although the terraces suggest a series of depositional stages.

2.2.3.3. **Reef limestones**

The shore of the area investigated is characterized by a series of almost continuous emergent reef terraces 0.5-8 km. wide. The most extensive of these stands 2 m. above sea-level. Others occur more discontinuously at 4, 7, and 9-10 m. These reefs are dissected in many places by stream erosion, but in general they are very fresh with little cementation of the calcarenite and calcirudite that fills the spaces between the coral colonies. Fossils are abundant and well preserved.

Table (2.2.): A Summary of Carella & Scarpa (1962) account of the stratigraphy of the Red Sea coastal plain.

Stratigraphy			**Maximum Thickness (m)**
Formation	**Age**	**Description**	
6. Abu Shagara	Quaternary	Reef limestones with intercalated coarse sands.	324
5. Dungunab	Post-Middle Miocene	Massive rock salt with minor anhydrite, gypsum, clays and sandstones (including a basalt flow 24 m thick).	722
4. Abu Imama	Middle Miocene	Reef limestones, calcareous mudstones and conglomerates.	137
3. Maghersum	Middle to Lower Miocene	(a) Marls, sandstones, conglomerates and Limestone.	111
		(b) Gypsum and anhydrite inter-bedded with sandstones and shales.	859
		(c) Rock salt with minor anhydrite.	465
2. Hamamit	Lower Miocene to Eocene	Coarse quartzitic sandstones (including 30 m of lava flow).	226
1. Mukawwar	Upper Cretaceous or Paleocene	Silty shales and sandstones.	190

2.3. Tectonic setting:

2.3.1. Introduction:

The Arabian-Nubian Shield (ANS) of north east Africa was formed by collision between east and west Gondwana. It represents the northern part of East African Orogeny (950- 550 Ma) which formed by the accretion of intra-oceanic arc/back-arc basin complexes as well as continental micro-Plates. The basement rocks of the ANS represents predominantly juvenile continental crust that was formed by differentiation of mantle melt largely without reworking of pre-existing continental crust. In northeast Sudan, the Nubian Shield is composed of a number of terrains including Gerf, Gabgaba, Gebeit, Haya and Tokar which are separated by E to NE trending ophiolite-decorated sutures formed during the Pan African Orogeny such as Hamisana Shear Zone, Oko Shear Zone and Nakasib Suture Zone.

2.3.2. Models of the Evolution of the Red Sea:

Many models have been proposed for the tectonic development of the red sea region prior to the present period of sea-floor spreading. Most of the models restricted the sea-floor spreading history to the last 10 Ma in the Gulf of Aden and to the last 5 Ma in the red sea.

2.3.2.1. Pure Shear Model by Mckenzie (1970)

Proposed that a period of diffuse extension prior to the beginning of sea-floor spreading is an essential part of rifting i.e. rifting was a result of lithospheric extension by faulting followed by mantle upwelling to maintain isostatic equilibrium. He assumed that the crustal and lithospheric extension was the same (uniform stretching). The stretching being symmetrical, and hence satisfies the condition of pure shear.

2.3.2.2. Simple Shear Model by Wernicke (1985)

The model is based on a low-angle normal fault (detachment) of regional extent that breaks away at the surface on the African continent and projects to sub-lithospheric levels beneath the Arabian continent (Wernicke, 1985; Voggenreiter et al, 1988).thus the extension is asymmetric both laterally and vertically. On the breakaway (footwall) side, deformation is intense at shallow crustal levels but crust and mantle deep beneath the detachment are not deformed. On the opposing side, the upper half of the lithosphere is undeformed whereas the deep lithosphere is highly extended by shear. This model also requires that the initial mantle upwelling be substantially offset from the surface position of the rift axis. As rifting proceeds the locus of mantle upwelling migrates up the dipping detachment surface to eventually coincide with the rift axis at the surface in the red sea. The position of the deep extension is eventually offset substantially from that at the surface.

2.3.2.3. **Diffuse Extension and Dyke Injection Model (Cochran, 1983)**

Cochran (1983) has reviewed all available evidence and has concluded that the presence of stretched, attenuated, down-faulted continental crust, as in McKenzie's (1978) model, best fits the evidence. Assuming a pre-sea floor spreading phase of diffuse extension and dyke injection (Cochran, 1983), where the frequency of injections increases towards the axis, the observed 20-30% basaltic dykes within the metamorphic unit exposed on Zabargad, located about 50 km from the axis, suggests that a large fraction of the crust in the transitional region might be basaltic, increasing towards the axis. Generation by "true" sea floor spreading is not implied by the presence of quasi- basaltic crust of this type.

This view can be reconciled with the amount of separation between Africa and Arabia required by plate reconstructions. Diffuse extension by faulting of the continental crust and by dyke injection, if lasting over a long enough period, can account for over 100 km widening of the basin (Cochran, 1983).

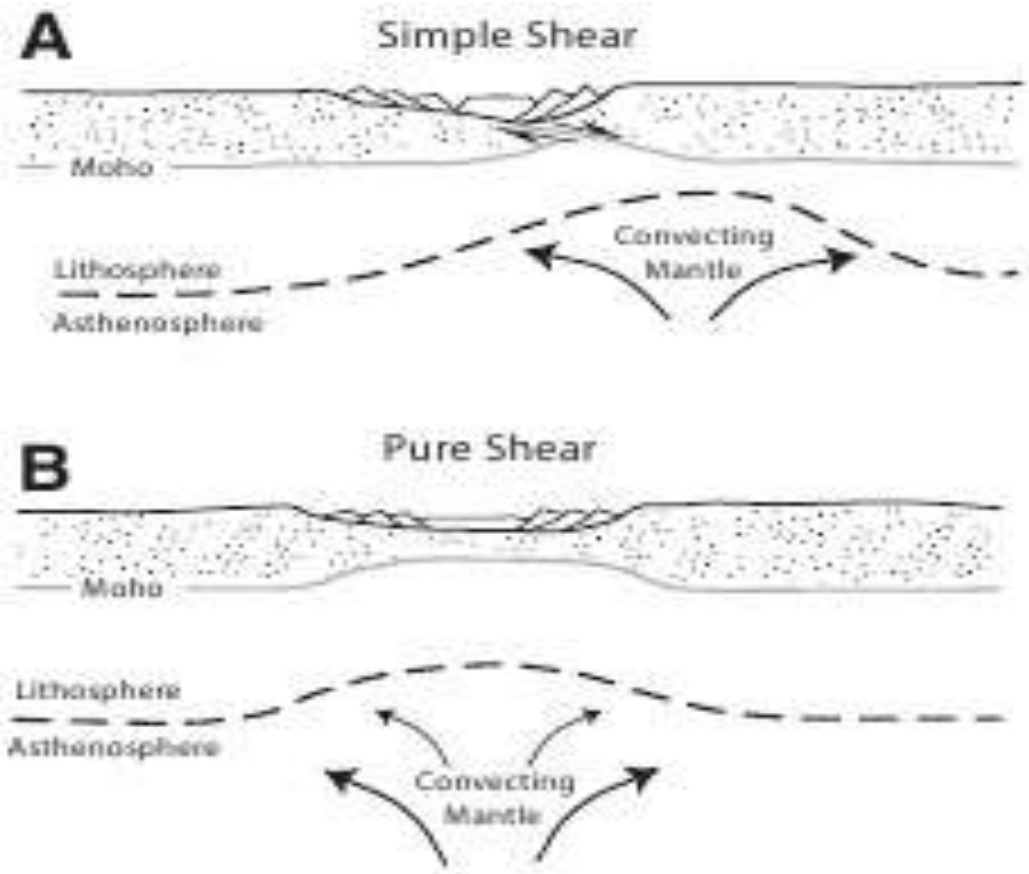

Fig (2.3.): A Simple shear model, B: Pure shear rift model. Models redrawn from Dixon et al.

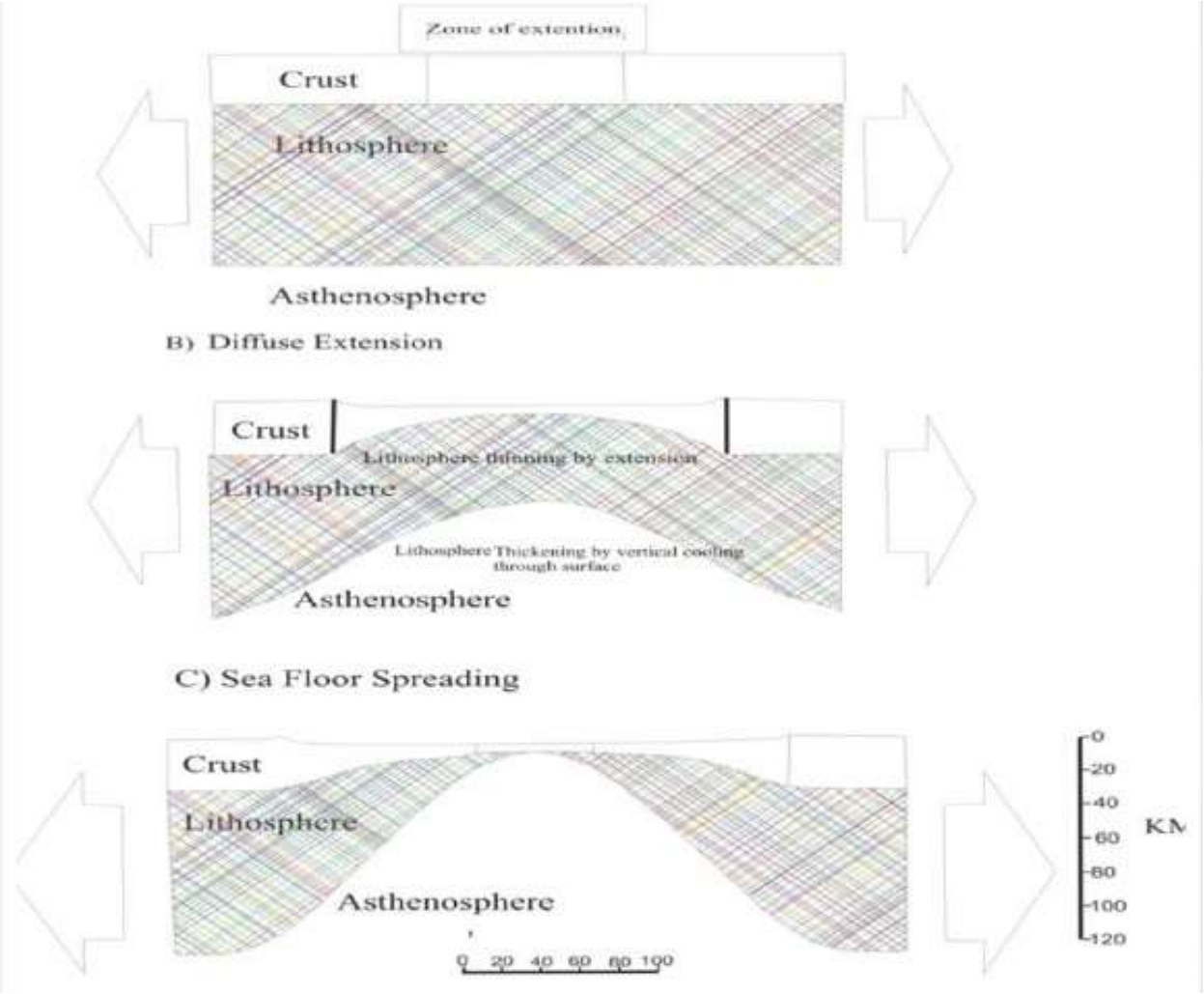

Fig (2.4.): Diffusion extension model of the Red Sea (*Cocharan, 1983*). When rifting begins.

2.3.2.4. **Two Stage Spreading Model Girdler and Styles (1974)**

According to Girdler and Styles (1974) and to Zitellini (1985), accretion of oceanic crust and sea floor spreading occurred in the southern Red Sea in two stages, the first taking place already at about 30 Ma. This view, based in part on the presence of magnetic anomalies along the margins of the Red Sea, implies that the entire width of the Red Sea is underlain by oceanic crust. Other authors interpret "marginal" magnetic anomalies as caused by basaltic dykes emplaced in the stretched continental crust, similar to those outcropping in the coastal areas of Saudi Arabia. This alternative view implies a southern Red Sea oceanic crust accretion limited to <5 Ma (Cochran 1983; Bonatti 1985).

Chapter three
Methods and Methodology

3.1. Remote sensing:

3.1.1. Historical background:

The period from 1960 to 2010 has experienced some major changes in the field of remote sensing. The background for many of these changes occurred in the 1960s and 1970s. Some of these changes are outlined below.

- First, the term "remote sensing" was initially introduced in 1960. Before 1960 the term used was generally aerial photography. However, new methods and technologies for sensing of the Earth's surface were moving beyond the traditional black and white aerial photograph, requiring a new, more comprehensive term be established.
- Second, the 1960s and 1970s saw the primary platform used to carry remotely sensed instruments shift from air planes to satellites. Satellites can cover much more land space than planes and can monitor areas on a regular basis.
- Third, imagery became digital in format rather than analog. The digital format made it possible to display and analyze imagery using computers, a technology that was also undergoing rapid change during this period. Computer technology was moving from large mainframe machines to small microcomputers and providing information more in graphic form rather than numerical output.
- Fourth, sensors were becoming available that recorded the Earth's surface simultaneously in several different portions of the electro-magnetic spectrum. One could now view an area by looking at several different images, some in portions of the spectrum beyond what the human eye could view. This technology made it possible to see things occurring on the Earth's surface that looking at a normal aerial photograph one could not detect.
- Finally, the turbulent social movements of the 1960s and 1970s awakened a new and continuing concern about the changes in the Earth's physical environment. Remotely sensed imagery from satellites - analyzed and enhanced with computers - made it possible to detect and monitor these changes. Thus, societal support was and continues to remain strong for this technology, even though very few people are familiar with the term, remote sensing.

3.2. **Geographic information system GIS:**

3.2.1. **Introduction:**

A geographic information system or geographical information system (GIS) is a system designed to capture, store, manipulate, analyze, manage, and present all types of spatial or geographical data. The acronym GIS is sometimes used for geographic information science (GIScience) to refer to the academic discipline that studies geographic information systems and is a large domain within the broader academic discipline of Geoinformatics. What goes beyond a GIS is a spatial data infrastructure, a concept that has no such restrictive boundaries.

In a general sense, the term describes any information system that integrates stores, edits, analyzes, shares, and displays geographic information. GIS applications are tools that allow users to create interactive queries (user-created searches), analyze spatial information, edit data in maps, and present the results of all these operations. Geographic information science is the science underlying geographic concepts, applications, and systems.

The first known use of the term "geographic information system" was by Roger Tomlinson in the year 1968 in his paper "A Geographic Information System for Regional Planning". Tomlinson is also acknowledged as the "father of GIS". There have been four distinct phases in the development of Geographic Information Systems. Phase one, between the early 1960s and the mid-1970s saw a new discipline being dominated by a few key individuals who were to shape the direction of future research and development. The second phase, from the mod 1970s to early 1980s saw the adoption of technologies by national agencies that led to a focus on the development of best practice. Phase three, between 1982 until the late 1980s saw the development and exploitation of the commercial market place surrounding GIS whilst the final phase since the late 1980s has seen a focus on ways of improving the usability of technology by making facilities more users centric.

GIS can relate unrelated information by using location as the key index variable. Locations or extents in the Earth space–time may be recorded as dates/times of occurrence, and x, y, and z coordinates representing, longitude, latitude, and elevation, respectively. All Earth-based spatial–temporal location and extent references should, ideally, be relatable to one another and ultimately to a "real" physical location or extent. This key characteristic of GIS has begun to open new avenues of scientific inquiry.

Geographic features can be categorized into two types, the discrete and the continuous data. The discrete data are the distinct features that have a location and shape and constitute spatially well-defined features (e.g. rivers, lineaments, dykes and house). The discrete data are generally represented in the vector format. Continuous data are borderless and non- distinctive values that change gradually (e.g. pollution zone, temperature and rainfall zonation).

3.3. **Gravity:**

3.3.1. **Introduction:**

Gravity is the force of attraction between masses. In geophysical terms it is the force due to the integrated mass of the whole Earth, which acts on the mechanism of a measuring instrument. Gravity methods have been used most extensively in the search for oil and gas, particularly in the twentieth century. Measurements are usually made at the surface of the Earth, in aircraft, on ships or in orbital satellite.

If the Earth were a perfect homogeneous sphere the gravity field would only depend on the distance from the center of the Earth. In fact the Earth is a slightly irregular oblate ellipsoid which means that the gravity field at its surface is stronger at the poles than at the equator. The mass (density) distribution is also uneven, particularly in the rigid crust, which causes gravity to vary from the expected value as the measurement position changes. These variations are expressed as gravity anomalies, the mapping of which gives us an insight into the structure of the Earth. Gravity Survey is a set of measurements of the gravitational field at a series of different locations over an area of interest. The objective in exploration work is to associate variations with differences in the distribution of densities and hence rock types, and therefore geologists can make inferences about the distribution of strata.

The primary goal of studying detailed gravity data is to provide a better understanding of the subsurface geology. The gravity method is a relatively cheap, non-invasive, passive and non- destructive remote sensing method.

3.3.2. **Theoretical background:**

Geophysical interpretations from gravity surveys are based on the mutual attraction experienced between two masses as first expressed by Isaac Newton. Newton's law of gravitation states that the mutual attractive force between two point masses “m1” and “m2” is proportional to one over the square of the distance between them. The constant of proportionality is usually specified as G, the gravitational constant. Thus, we usually see the law of gravitation written as shown to the right where F is the force of attraction, G is the gravitational constant, and r is the distance between the two masses, m1 and m2.

$$F = \frac{Gm_1m_2}{r^2}$$

3.3.3. **Gravitational acceleration:**

When making measurements of the earth's gravity, we usually don't measure the gravitational force (F). Rather, we measure the gravitational acceleration (g). The gravitational acceleration is the time rate of change of a body's speed under the influence of the gravitational force. That is, if you drop a rock off a cliff, it not only falls, but its speed increases as it falls. In addition to defining the law of mutual attraction between masses, Newton also defined the relationship between a force and acceleration. Newton's second law states that force is proportional to acceleration. The constant of proportionality is the mass of the object.

Combining Newton's second law with his law of mutual attraction, the gravitational acceleration on the mass m2 can be shown to be equal to the mass of attracting object, m1, over the squared distance between the center of the two masses, r.

$$F = m_2 g \ , \ g = \frac{G m_1}{r^2}$$

3.3.4. **Units associated with gravitational acceleration:**

Acceleration is defined as the time rate of change of the speed of a body. Speed, sometimes incorrectly referred to as velocity, is the distance an object travels divided by the time it took to travel that distance (i.e., meters per second (m/s)). Thus, we can measure the speed of an object by observing the time it takes to travel a known distance.

If the speed of the object changes as it travels, then this change in speed with respect to time is referred to as acceleration. Positive acceleration means the object is moving faster with time, and negative acceleration means the object is slowing down with time. Acceleration can be measured by determining the speed of an object at two different times and dividing the speed by the time difference between the two observations. Therefore, the units associated with acceleration is speed (distance per time) divided by time; or distance per time per time, or distance per time squared.

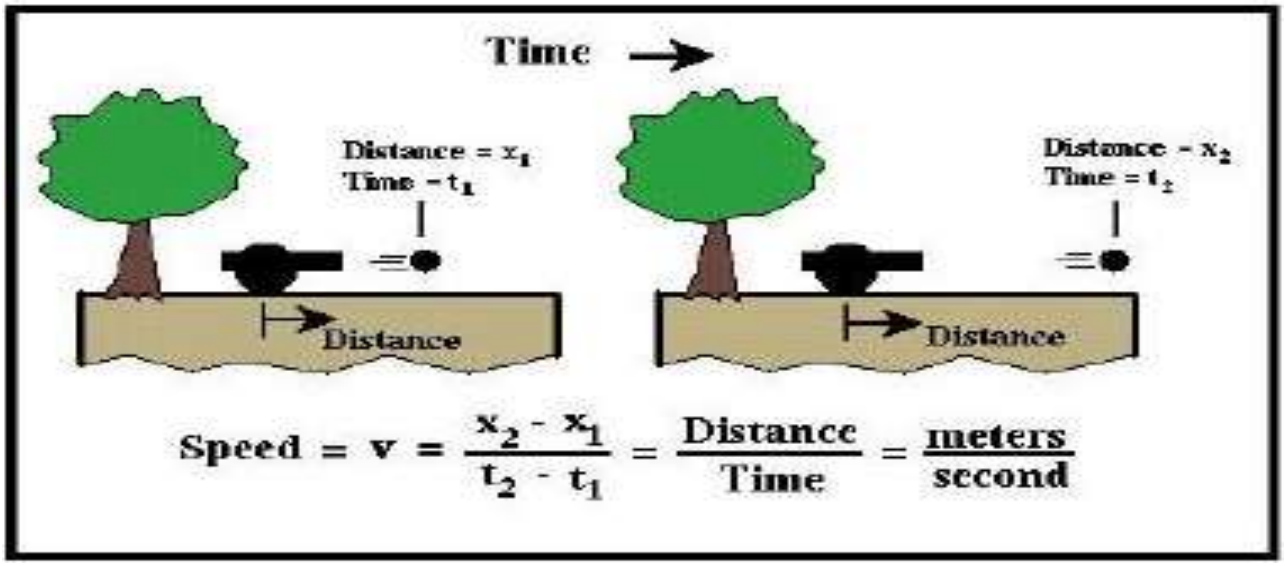

If an object such as a ball is dropped, it falls under the influence of gravity in such a way that its speed increases constantly with time. That is, the object accelerates as it falls with constant acceleration. At sea level, the rate of acceleration is about 9.8 meters per second squared. In gravity surveying, we will measure variations in the acceleration due to the earth's gravity. Variations in this acceleration can be caused by variations in subsurface geology. Acceleration variations due to geology, however, tend to be much smaller than 9.8 meters per second squared. Thus, a meter per second squared is an inconvenient system of units to use when discussing gravity surveys.

The units typically used in describing the gravitational acceleration variations observed in exploration gravity surveys are specified in milliGals. A Gal is defined as a centimeter per second squared. Thus, the Earth's gravitational acceleration is approximately 980 Gals. The Gal is named after Galileo Galilee. The milliGal (mgal) is one thousandth of a Gal. In milliGals, the Earth's gravitational acceleration is approximately 980,000.

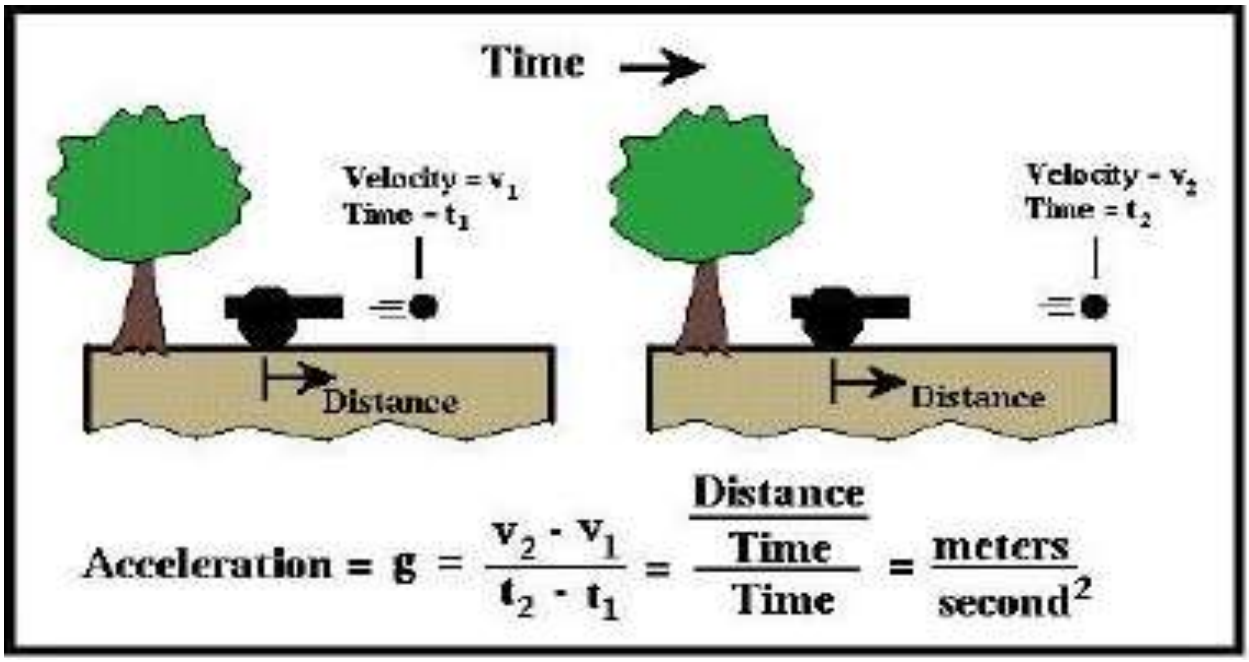

3.3.5. **The relationship between gravitational acceleration and geology:**

Density is defined as mass per unit volume. For example, if we were to calculate the density of a room filled with people, the density would be given by the average number of people per unit space (e.g., per cubic foot) and would have the units of people per cubic foot. The higher the number, the more closely spaced are the people.

Thus, we would say the room is more densely packed with people. The units typically used to describe density of substances are grams per centimeter cubed (gm/cm^3); mass per unit volume. In relating our room analogy to substances, we can use the point mass described earlier as we did the number of people.

Consider a simple geologic example of an ore body buried in soil. We would expect the density of the ore body, d2, to be greater than the density of the surrounding soil, d1.

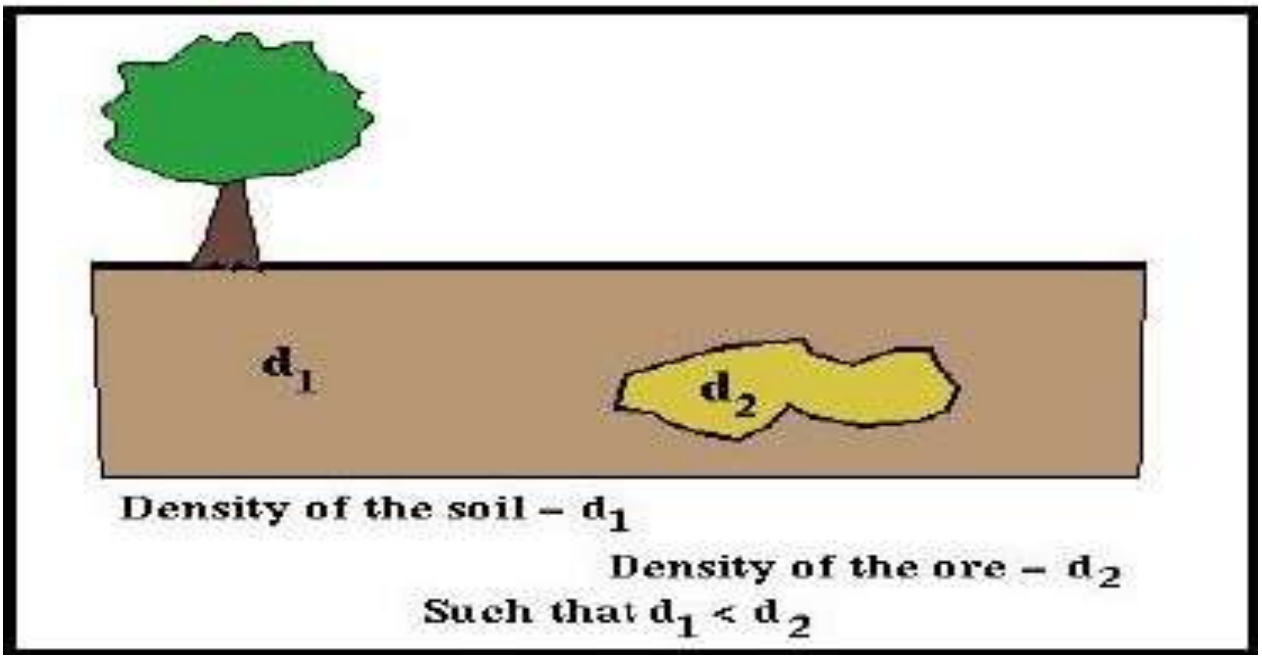

In this part we assume that all of the point masses have the same mass.

As the ball is dropped from a ladder, the size of the acceleration the ball undergoes will be proportional to the number of close point masses that are directly below it. We're concerned with the close point masses because the magnitude of the gravitational acceleration varies as one over the distance between the ball and the point mass squared. The more close point masses there are directly below the ball, the larger its acceleration will be.

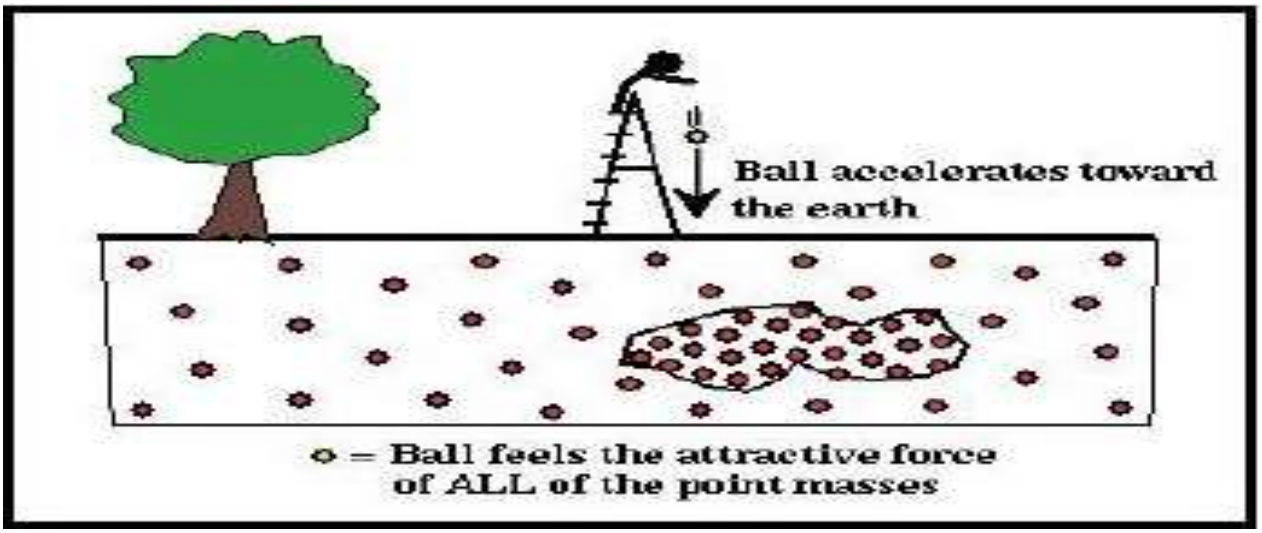

We could, therefore, drop the ball from a number of different locations, and, because the number of point masses below the ball varies with the location at which it is dropped, map out differences in the size of the gravitational acceleration experienced by the ball caused by

variations in the underlying geology. A plot of the gravitational acceleration versus location is commonly referred to as a "gravity profile".

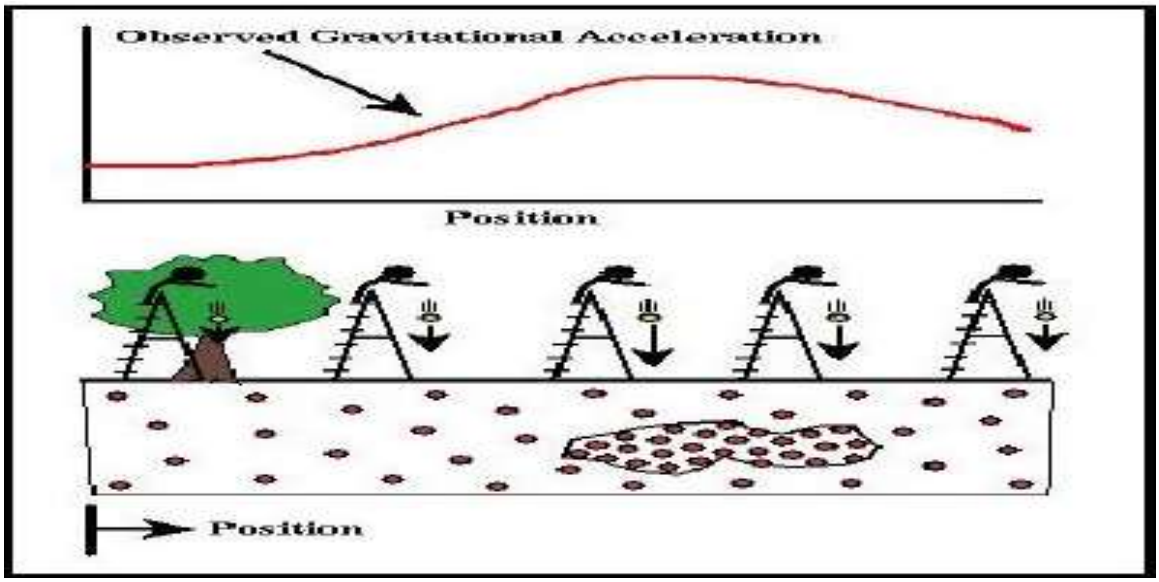

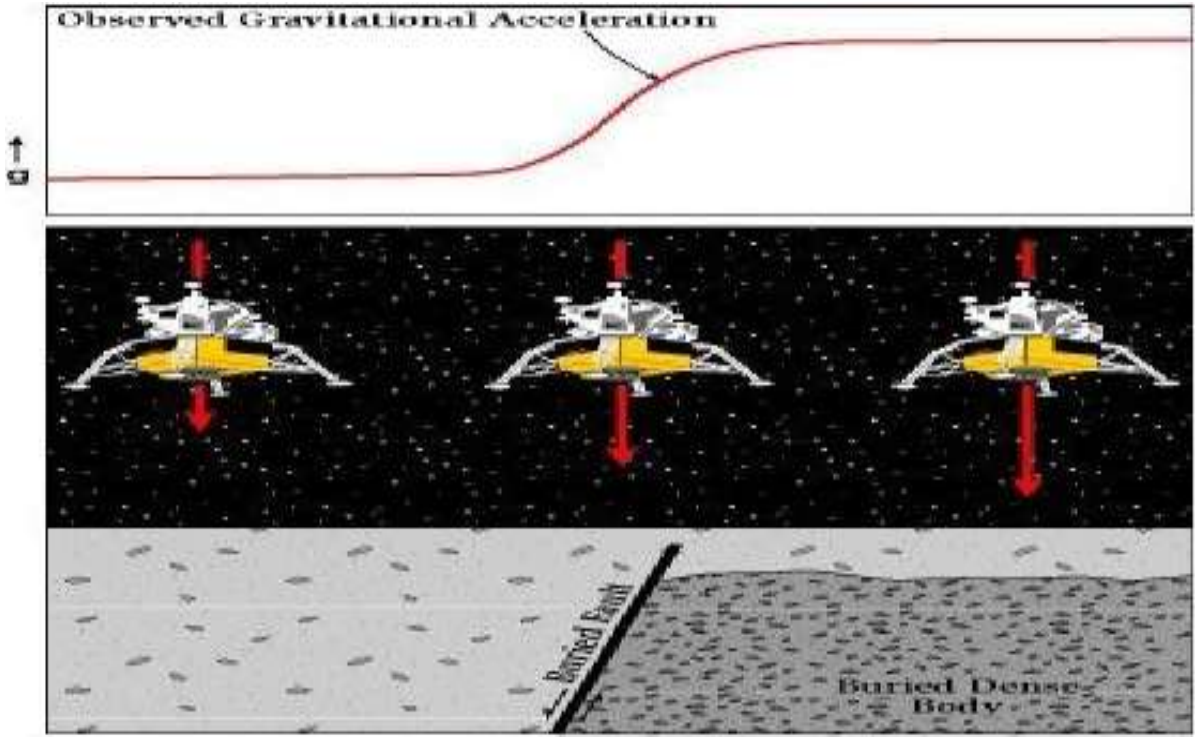

3.3.6. **Density contrast:**

3.3.6.1. **Variation with geology**

The shape of the curve describing the variation in gravitational acceleration is not dependent on the absolute densities of the rocks. It is only dependent on the density difference (usually referred to as density contrast) between the ore body and the surrounding soil. That is, the spatial variation in the gravitational acceleration generated from our previous example would be exactly the same if we were to assume different densities for the ore body and the surrounding soil, as long as the density contrast, d2 - d1, between the ore body and the surrounding soil were constant. One example of a model that satisfies this condition is to let the density of the soil be zero and the density of the ore body to be d2 - d1.

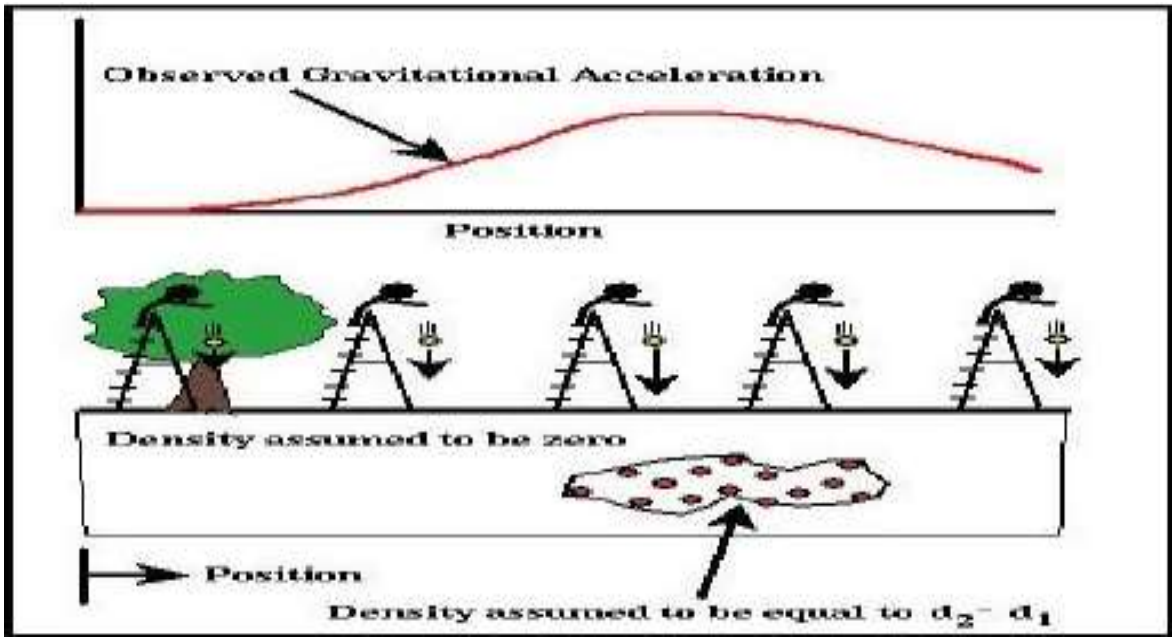

Thus far it sounds like a fairly simple proposition to estimate the variation in density of the earth due to local changes in geology. There are, however, several significant complications. The first has to do with the density contrasts measured for various earth materials.

The densities associated with various earth materials are shown below:

Material	Density (gm/cm^3)
Air	~0
Water	1
Sediments	1.7-2.3
Sandstone	2.0-2.6
Shale	2.0-2.7
Limestone	2.5-2.8
Granite	2.5-2.8
Basalts	2.7-3.1
Metamorphic Rocks	2.6-3.0

Table (3.1.): The densities associated with various earth materials.

3.3.6.2. Variation with latitude

This is needed because of the ellipticity of Earth "g" is reduced at low latitudes because of the Earth's shape and because of rotation:

Lat. correction = Gst. – Gφ, whereas "Gφ" is the Theoretical Gravity.

The formula for the general increase of (g) with latitude (θ), based on the most recently accepted spheroid approximation, is given by:

$$g = 97803\ 1.8\ (1 + 0.0053024 \sin 2\ \theta - 0.0000058 \sin 2\ 2\theta)$$

Where g is the predicted value of gravity at latitude (θ) and 978031.8 is the value of gravity at the equator. The equation with the above constants is also known as the International Gravity Formula 1967. This equation includes both the Newtonian attraction of the Earth as a spheroid and the centrifugal force caused by its rotation about its axis.

3.3.6.3. Variation with elevation

3.3.6.3.1. Bouguer correction

This accounts for the mass of rock between the station and sea level. It has the effect of increasing g at the station, and thus it is subtracted.

The formula for the Bouguer correction on land is:

$$BC = 2\pi\ G\ \rho\ h = 4.185 \times 10\text{-}5\ \rho \sim 0.1\ \text{mGal/m}$$

Where h = height above sea level and ρ = density. This is also the formula for an infinite slab of rock. The Bouguer correction is subtracted on land, but at sea it must be added to account for the lack of mass between the sea floor and sea level:

$$BC_{sea} = 2\pi G (\rho_{rock} - \rho_{water}) h, \text{ where } h = \text{water depth.}$$

It is possible to combine the Free Air and Bouguer corrections:

$$BC\&FAC = [2g/r - 2\pi G\rho] h$$

3.3.6.3.2. Free-air correction

It is necessary to correct for the variable heights of the stations above sea level, because g falls off with height. It is added:

$$FAC = 2g/r = 0.3086 \text{ mGal/m}$$

3.3.6.3.3. Terrain correction

The effect of terrain is always to reduce observed g. This is true for a mountain above the station and a valley below the station, which both cause g to be reduced. Terrain corrections are done by hand using a transparent graticule, or by computer if a digital terrain map is available. The graticule is placed on a map and the average height of each compartment estimated. A "Hammer chart" is then used to obtain the correction. This chart gives the correction for a particular distance from the station. It has been worked out assuming a block of constant height for each compartment. Other charts are available, e.g., the Sandberg tables, which provide for larger terrain differences and assume sloping terrain. Terrain corrections are now done with digital terrain maps and a computer program if possible, as doing the work by hand is very time consuming and involves a lot of repetition.

3.3.6.4. Tidal correction

This is necessary for:

I. Ultra-accurate surveys where it is not sufficiently accurate to absorb the effect of the sun and moon in the drift correction, and
II. If gravimeter drift is low and the base station tie backs were made with a similar period as the tides.

Tides occur both in the solid Earth and the sea. The latter is important for marine surveys. The period of the tides is about 12 hrs. The amplitude of the gravitational effect of the solid Earth tides is up to ~ 0.3 mGal throughout the day at a fixed point on Earth.

3.3.6.5. **Drift correction**

A graph is plotted of measurements made at the base station throughout the day. Drift may be non-linear, but it has to be assumed that it is be linear between tie backs for most surveys. The drift correction incorporates the effects of instrument drift, uncompensated temperature effects, solid Earth and sea tides and the gravitational attraction of the sun and moon.

3.3.6.6. **Calibration of the meter**

This is a number provided by the manufacturer that translates scale readings into mGal:

(Actual reading +drift –base reading) calibration = Gst. – Gbase

3.3.7. **Gravity anomalies:**

3.3.7.1. **Bouguer anomaly (B.A)**

The B.A is equivalent to stripping away everything above sea level. It is the anomaly most commonly used in prospecting.

The equation for the Bouguer anomaly is:

$$BA = gobs - g\,\varphi + FAC \pm BC + TC\ (\pm EC)$$

3.3.7.2. **Free-air anomaly (F.A.A)**

The F.A.A may be thought of as squashing up all the mass above sea level into an infinitesimally thin layer at sea level, and measuring gravity there. The FAA is mostly used for marine surveys and for investigating deep mass distribution, e.g., testing theories of isostasy.

The equation for F.A.A is:

$$FAA = gobs - g\,\varphi + FAC\ (\pm EC)$$

Chapter Four

Data Acquisition and Processing

4.1. Introduction:

The present work various data types, from different sources, that individually constitute part of the spatial information system pertaining to the northern Red Sea area have been used. In the next sections the basic data characteristics and data processing will be considered. Geophysical data available to this work were obtained in a form of gravity data. On the other hand the remote sensing data include: Operational Land Imager (OLI) scenes and Digital Elevation Model (DEM) were available in digital GEO-TIFF format. Additional descriptive data or attributes such as surface geological data and wells available in this work.

4.2. Dataset:

The following datasets were used in this study:

Geophysical Datasets	Remote Sensing Datasets	Geological Information
• Gravity	• OLI • DEM	• Geological maps • Literature

4.2.1. Remote Sensing:

Landsat 8 OLI comprises 11 bands. Images consist of nine spectral bands with a spatial resolution of 30 meters for Bands 1 to 7 and 9. New band 1 (ultra-blue) is useful for coastal and aerosol studies. New band 9 is useful for cirrus cloud detection. The resolution for Band 8 (panchromatic) is 15 meters. Thermal bands 10 and 11 are useful in providing more accurate surface temperatures and are collected at 100 meters. Approximate scene size is 170 km north-south by 183 km east-west. Red sea area is covered by the following Landsat OLI Imageries: path 171, row 46 and path 171, row 45.

4.2.2. Geographic Information System:

In this study, remote sensing techniques were used together with the field geological data in the GIS framework to generate the final geological map of the study area.

Geological mapping has been increasingly supported by the use of remote sensing and GIS techniques, which improve the quality and timely availability of basic information for exploration activities. Based on their spectral signatures in different Color composite imageries,

the discriminated lithological units represent the geological units of the map area. The Geo-database facilitate the use of the integrated various data as registered multi-layers.

4.2.3. **Acquisition and reduction of gravity data:**

The gravity data of the Red Sea was obtained from the Satellite Geodesy at the Scripps Institution of Oceanography, University of California San Diego. These data were compiled to produce a Bouguer anomaly map, residual anomaly map, 1^{st} & 2^{nd} vertical derivatives maps, and 1^{st} & 2^{nd} horizontal derivatives maps. Bouguer reduction density was 2 .67 gm/cm3.

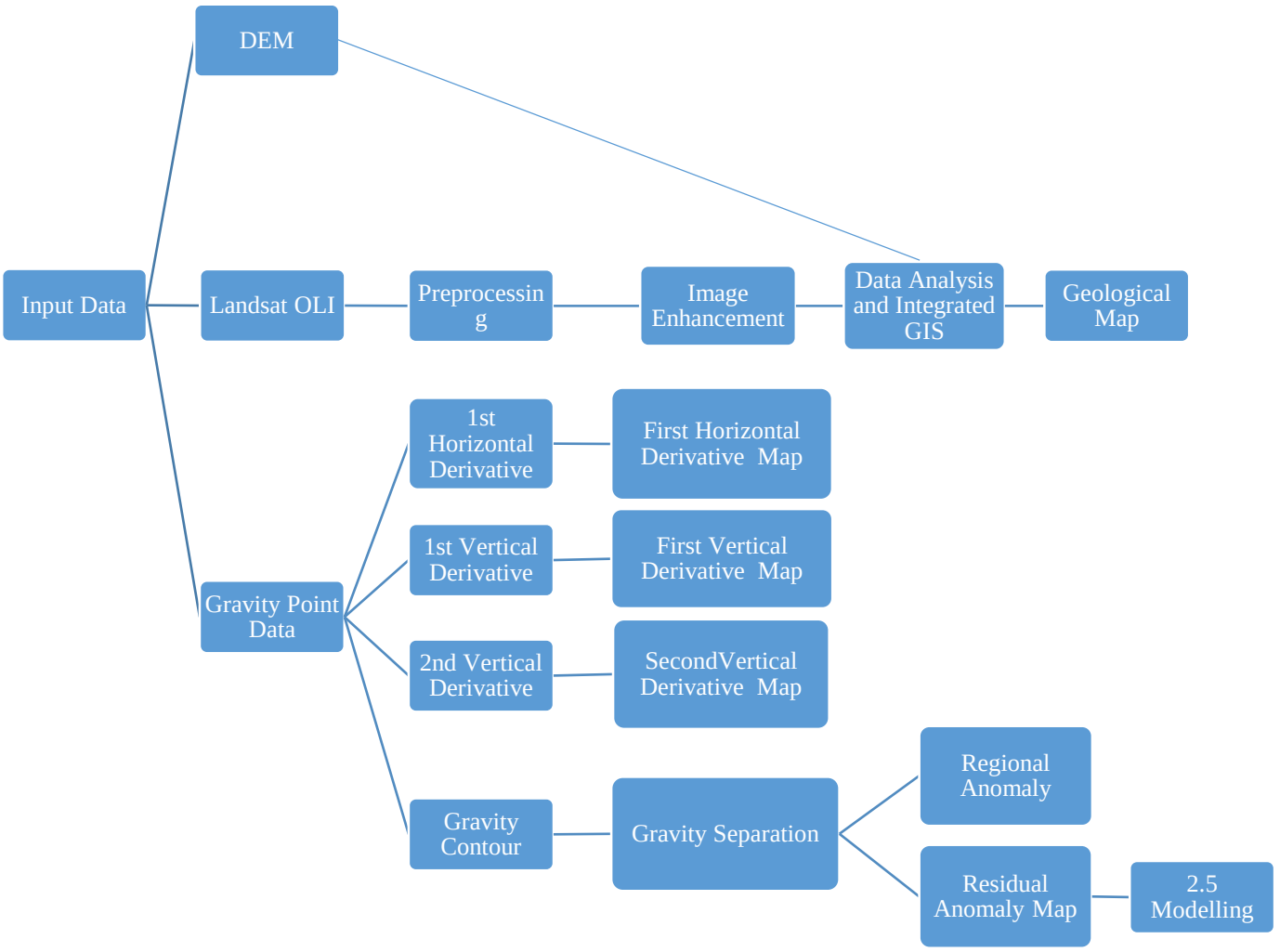

Fig (4.1.): Flow chart of the methodology adopted in the present study.

Chapter Five

Results and Interpretation

5.1. Remote Sensing:

5.1.1. Digital Image Processing:

Digital image processing is the manipulation of digital data by computer programs in order to improve the appearance of an image (Gibson, 2000).

5.1.1.1. Pre-processing Techniques (Image Preparation)

The image preparation for the present study included the following steps:

5.1.1.1.1. Haze Correction

Pixel brightness values recorded by the sensors on the satellite contain errors caused by atmospheric scattering of the light rays on their path from the sun to earth surface and back to the satellite. The amount of this error differs from one band to another. The amount of scattering depends on the wavelength of the band and the atmospheric condition (Sabins, 1996). The Atmosphere partially scatters the shorter wavelengths of light, which cause haze and produce low contrast image. With the Atmospheric Correction Module, we can accurately compensate for atmospheric effects. The Atmospheric Correction Module provides two atmospheric correction modeling tools for retrieving spectral reflectance from multispectral and hyperspectral radiance images: Quick Atmospheric Correction (QUAC) and Fast Line-of-sight Atmospheric Analysis of Spectral Hypercubes (FLAASH). In this study we used FLAASH technique.

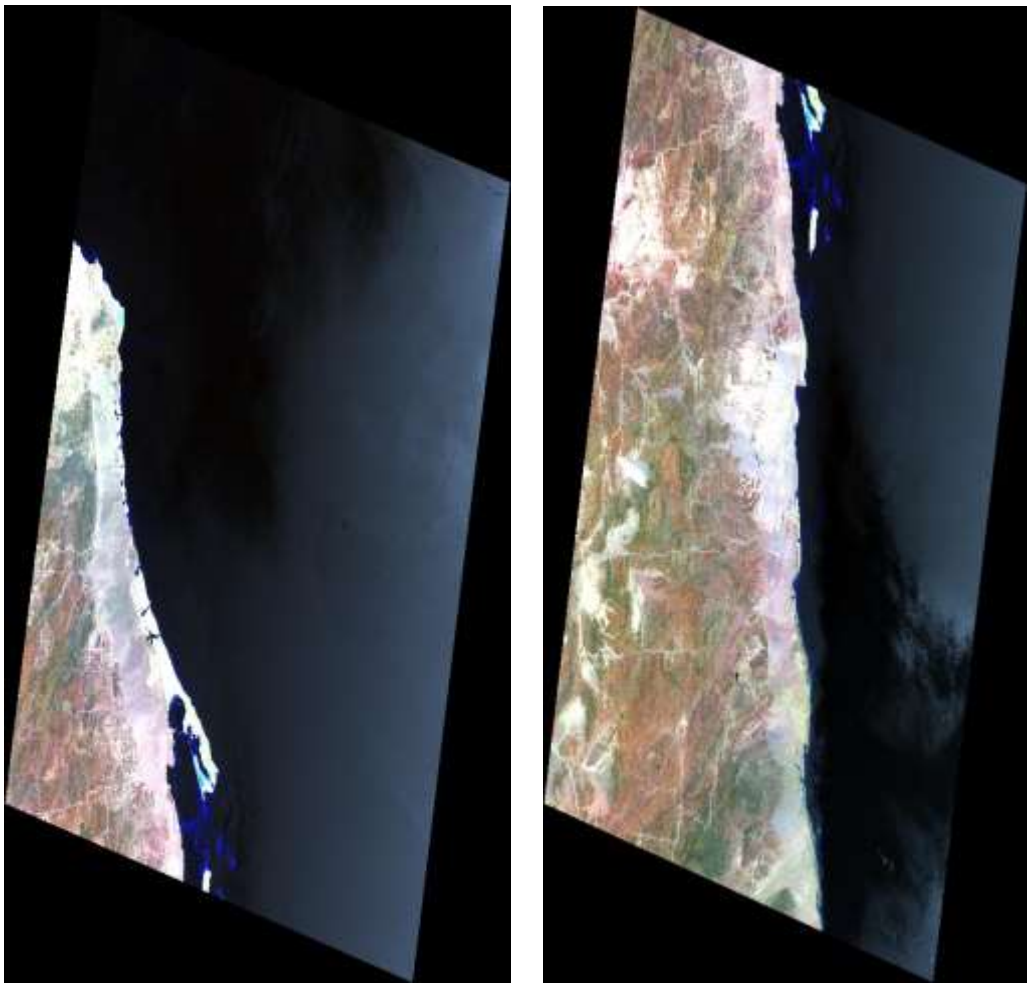

(A) (B)

Plate (5.1. A) Represents FLAASH version of Scene path 171, raw 45.

Plate (5.1. B) Represents FLAASH version of Scene path 171, raw 46.

5.1.1.1.2. **Digital Mosaic**

The regional coverage of individual Landsat images can be extended by combining adjacent images into a mosaic, which required uniform scale and minimum distortions before combination and this makes mosaic combination easier (Sabins, 1996). If the two images pertain in different seasons or time, the mosaic will give sharp radiometric boundary between two images (Gupta, 2003).

Plate (5.2.) Shows a digital mosaic of reflectance bands of Scene 171-45 and Scene 171-46.

5.1.1.1.3. **Image Subsetting**

Spatial subsetting was performed on the raw digital images including band 1, 2, 3, 4, 5, 6, 7 & 8 in order to spatially resize the image to the following coordinates: lat. 20° 19' 35.1"N _ 21° 34' 20.5" N and long. 36° 53' 37.92" E _ 37° 12' 47" E.

Plate (5.3.) Demonstrates a subset of the study area deducted from the mosaic image of the reflectance bands.

5.1.1.2. **Color Composite**

High spectral resolution is important when producing Color composite images The rule of Color composites is to set the most informative band for a particular purpose in the red, the next in green and the least informative band in blue (Drury, 1993). The different (RGB) combinations discriminate the rock types which is useful in geological application.

(A) (B)

Plate (5.4. A) Landsat OLI color composite obtained using bands 6, 5, 3 in RGB, respectively.

Plate (5.4. B) Landsat OLI color composite obtained using bands 7, 5, 6 in RGB, respectively.

Different features observed in Plate No (5.4. A), such as the black color of water, Pale green color of carbonates outcrop, blue color of reefs, light brown Color of the Wadi deposits and alluvial fan and also the dark brown and other green colors of the basement complex. Another Color composite was prepared using the infrared bands of the image set. It was composed employing bands 7, 5, 4 in RGB, respectively (plate 5.4. B). This band combination is termed the infrared image.

5.1.1.3. **Resolution enhancement**

Image sharpening was used to automatically merge the low resolution multispectral band with the high-resolution grayscale band (with resampling to the high-resolution pixel size). Pan Spectral Sharpening technique was used as a tool for the sharpening process. The multispectral data was automatically resampled to the high resolution pixel size using a nearest

neighbor convolution method. So the image set of the study area sub-scene has the pixel size of the input high-resolution data and the same spectral resolution as of the multispectral data set.

Plate (5.5.) Pan Sharpening in Landsat OLI obtained using band 7, 5, 2 in RGB, respectively.

On this image, the color composite image of OLI band 7, 5 and 2 in (RGB) with resolution 30 m, converted to high spatial resolution image (resolution 15 m) based on band 8 by Gram-Schmidt Pan Sharpening transformation.

5.1.1.4. **Contrast Stretching**

Contrast stretching modifies the grey scale to produce a more interpretable image (Sabins, 2000). It is so happens that the number of actually recorded intensity levels in the scene is rather low and the full dynamic range of the digital image (256 levels) is not fully utilized. It is worth mentioning that contrast stretching was applied in this study after various digital processing procedures to enhance the resulting image, and was not applied as a separate enhancement process.

5.1.1.5. **Band Ratio**

Spectral band rationing is a proven technique which allows identification of geological materials based on the reorganization of diagnostic absorption bands. It minimizes the effect of topographic slope, aspect, and Albedo differences between rocks, and enhances the subtle differences in reflectivity between bands which are diagnostic of various surface materials. Ratio images are prepared by dividing the DN value in one spectral band by the corresponding DN value in another band for each pixel. Band ratio technique is applied to extract information not really seen in single image (Gupta, 2003)

The individual ratio images (bands 6/7, 4/2 and 5/6 * 4/5) are used in lithological Discrimination of different rock types in the study area.

The ratio images of color composite are correlated with color image of individual OLI bands, which express more geological information and have greatest contrast between units. ratio of band 4/2 enhance the image and give pixels of iron bearing rocks a higher value than those composed of pure quartz, band ratio 6/7 is for clays and carbonates (Drury, 1993) .

Band ratio 6/7, 6/2, 4/2, and 4/5 have been computed which express more geological information and give greatest contrast between rocks units. Based on the above assumptions, the technique was used to produce a false Color composite image using combinations of ratios 6/7, 6/5 and 4/2 in R, G and B, respectively. This image is called Abrams's image (Abrams et al., 1983).

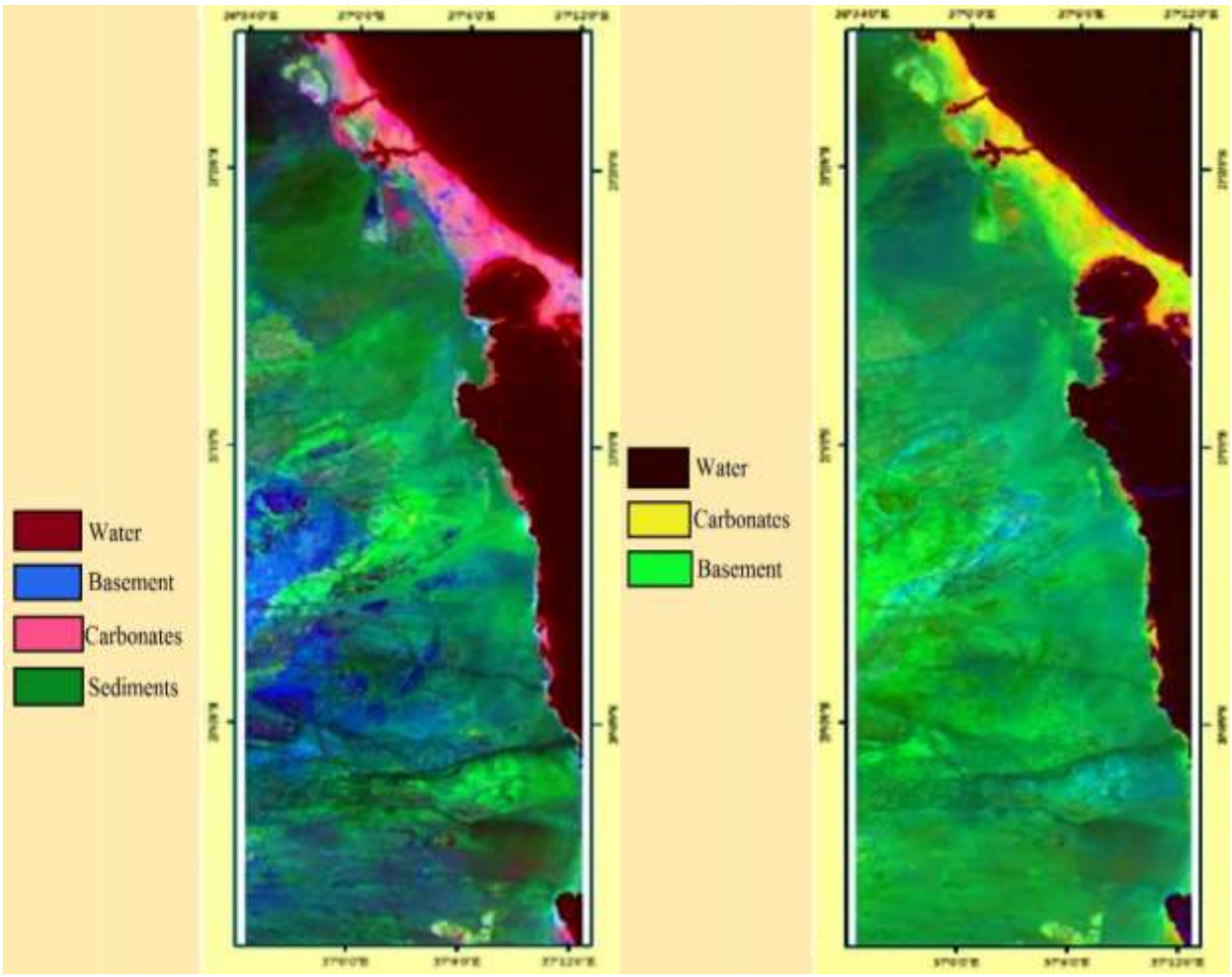

(A) (B)

Plate (5.6. A) Ratio image obtained using the following band ratio combination: (band6/band 7), (band 6/band 5) and (band 4/ band 2) assigned to red, green and blue, respectively.

Plate (5.6. B) Sultan ratio image Color composite obtained using band ratios 6/7, 6/2, (6/5*4/5) in RGB (Sultan et al., 1987), respectively.

In Plate (5.6. A) different features observed in this Plate such as the very light violet color of the carbonate outcrop, the light green of the wadi deposits and alluvial fan, and the very dark violet of the upper clastic group and basement complex.

In Plate (5.6. B) different features observed in this Plate such as the very dark yellow color of the carbonate outcrop, dark violet color of the reefs and the green Color of the upper Clastic group and basement complex.

5.1.1.6. **Principal Components Analysis**

Principal component analysis often called PCA, Principal component analysis is a multi-variant statistical technique commonly used in a digital image processing of remotely sensed data (e.g. Singh and Harrison, 1985; Loughlin, 1991; Eklundh and Singh, 1993; Chavez and Kwarteng, 1989; Roger, 1996 and Kenea, 1997).

The transformation of the raw data using PCA can result in new principal component images that are more interpretable than the original data (Jensen, 1996). The PCA is used to compress the information content of a number of bands of imagery or to reduce the dimensionality from a number of bands to two or three PCs (Jensen, 1996). It is also used to reduce the redundancy of information in highly correlated image set.

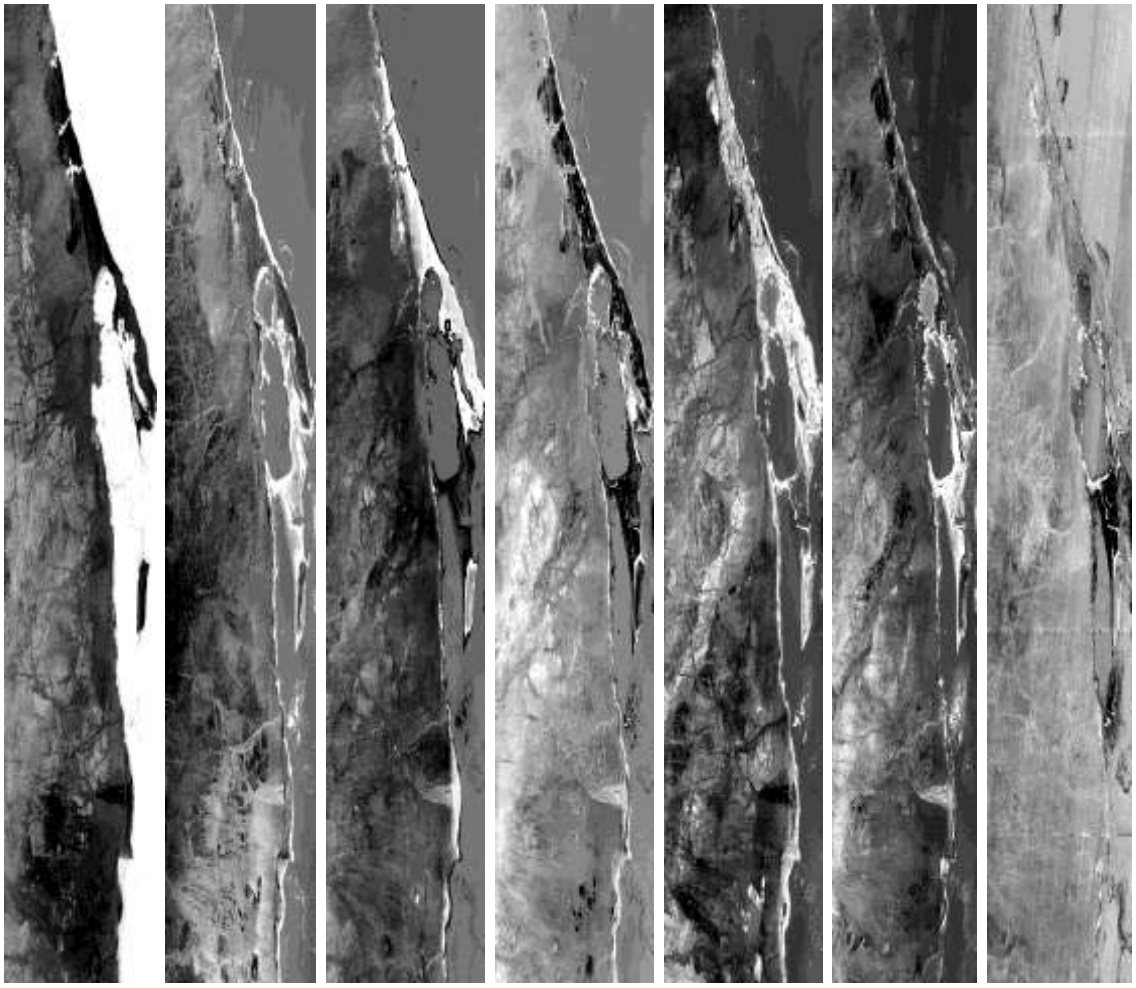

A B C D E F G

Plate (5.7.) From A to G seven principal component images obtained transforming the seven reflective OLI bands.

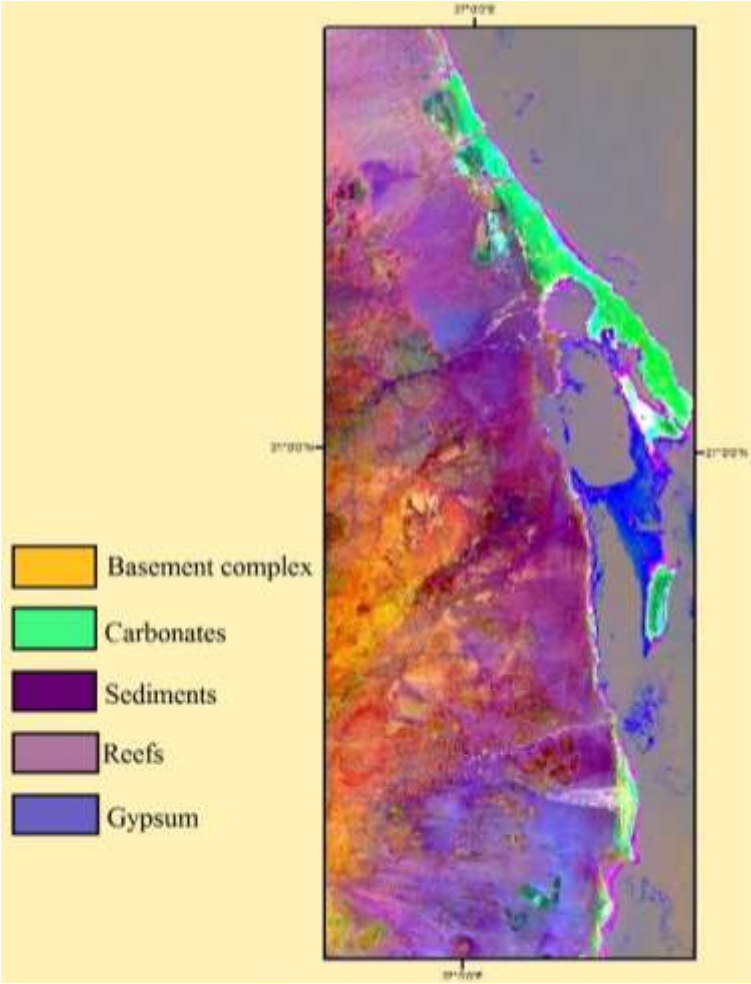

Plate (5.8.) Principal Component analysis color composite obtained by assigning PC2, PC3, and PC4 to RGB, respectively.

In plate (5.7. A) The contrast was increased and many criteria such as topography, lithology, structural features and drainage patterns are clear and discernible. Image plate (5.7. I B) has low contrast than that of PC2, also topography and lithology has less expressions. PC3 image has low contrast than that of PC2, also topography and lithology has less expressions. Image plate (5.7. I C) contains information about drainage system but no lithological or topographic expressions can be discerned. Image plate (5.7. I D&E) outlined only the vegetation cover in the area in dark tones, while Image plate (5.7. I F) is assumed to contain only noise.

In plate (5.7. II), the carbonates outcrops are reddish color. The gypsum quarries is located at the center of the image are light blue color, the reefs appear to be very light blue color and basement complex are light violet color.

5.1.2.**Geological map of the study area:**

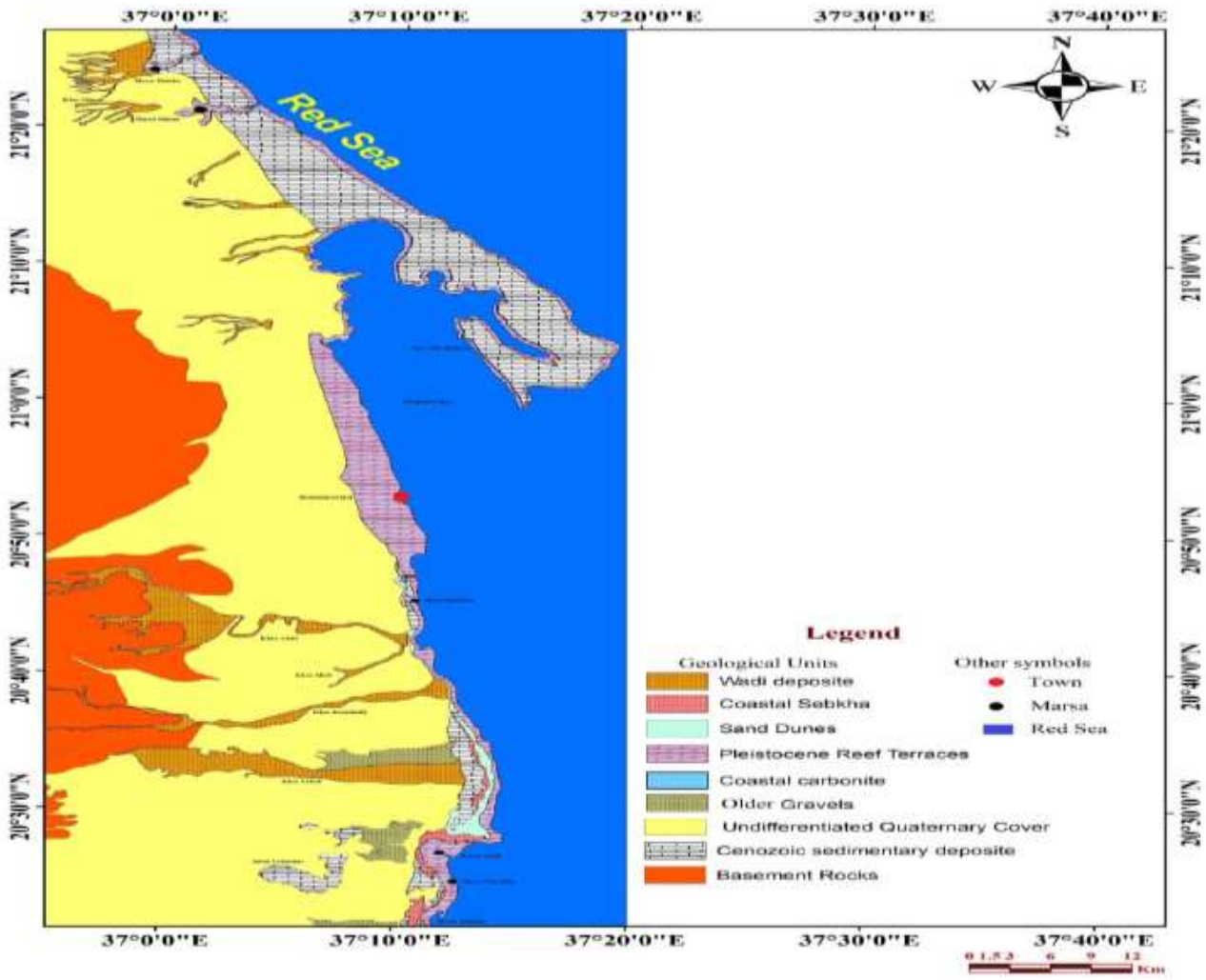

Fig (5.1.): Showing the geological map of study area.

5.2. **Gravity:**

5.2.1. **Qualitative interpretation:**

The qualitative interpretation involves the description of the resulting anomaly of gravity data, and the explanation of the major features revealed by these data in terms of types of likely geological formations and structures. The main feature of Bouguer anomalies over the coastal plain see Fig (4.2.) may be summarized as follows: The regional gravity gradient increases east ward increase and north wards has a maximum value on the eastern part of Abu Shagara Peninsula (Carbonate sediment). While the maximum anomaly gradient over the basement is fairly constant (2.4 to 2.6 mGal/km),Over the sediments it is higher and increases north wards from (3.9 mGal/km to 6.0 mGal/km) is chosen to compute the gravity effect of sediments A computer method (Written by Qureshi & Mula) based on two dimensional mass distribution (Talwani et al 1959.). The gravity effect of the sediments reaches 38mgal in the region of Dungunab Bay. The gravity low over the Red Sea Hills has been interpreted by a thickening of the underlying crustal layers in accordance with the Airy concept. However that lithosphere beneath the Hills has thinned (though not as much as under the Red Sea). (Girder et al .1969). Many faults were identified from the map Fig (5-2) indicated by dense gradient belt of gravity anomaly, distortion zone of gravity anomaly contours and borderline of significant positive gravity anomaly and negative one. Some of the identified faults are main faults but some of them are just minor faults with limited effects, the main faults which separate the gravity high area trending NS, the other faults trending NW to SE and NE to SW.

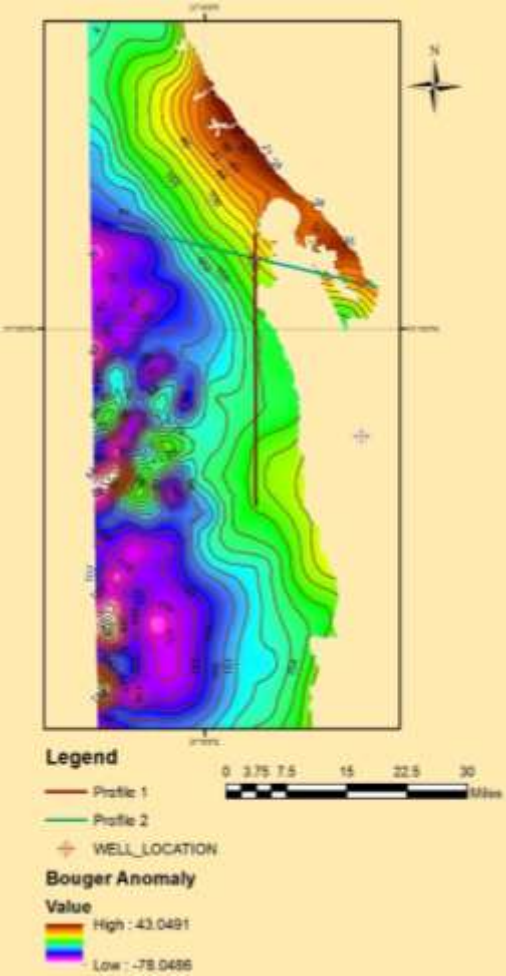

Fig (5.2.): Showing Regional Bouguer Gravity map for Northern Red Sea region. Contour interval is 4mGal. Crosses lines are gravity model profiles (1 & 2).

5.2.2. **Quantitative interpretation:**

5.2.2.1. **Regional- Residual Separation**

The problem of the regional and residual anomalies arises in all geophysical methods which are based on measurements of a potential field. Basically the question is that of separating a potential field into possible component parts and of ascribing separate geological causes to these parts. The determination of a satisfactory regional is a geological as well as a geophysical problem Nettleton, (1954). Grant, (1954) defined the regional gravity anomaly as "the field that is too broad to suggest the object of exploration and it is generally assumed to be smooth and regular, suggesting characteristically the field due to a deep-seated disturbance". Nettleton, (1954) adopted the following definition: "the regional is what you take out to make what is left looks like the structures". Paul, (1967) defined it as “the regional field is the field that would be Produced when local anomalous masses are replaced by masses of the same density as that of the country rocks. This definition will smooth out the regional field sufficiently and also

will signify the residuals as the field due to local mass distributions with densities equal to density contrasts i.e. true densities minus the densities of the surroundings". Skeels (1967), defined the regional gravity as “the interpreter's concept of what the Bouguer gravity should be if the anomalies were not present" and the residual gravity as "what remains of Bouguer gravity after subtraction of a smooth regional effect". However, the residual can be expressed as follows:

Residual gravity = Observed gravity - Regional gravity

5.2.2.1.1. Polynomial fitting method

This is a pure analytical method in which matching of the regional by a polynomial surface of low order exposes the residual features as random errors (Telford et al 1976). This method assumes the residuals to be random errors whose sum is zero. Thus the analytical residual is composed of positive and negative parts. The polynomial equation has the form:

$$y = a + bx + cx2 + dx3$$

Where a, b, c and d, are coefficients.

The polynomial order is the largest power of x in the equation. For fitting a data point (xi, Yi), it assumes that all of the errors occur in the measured (y) values and there are no errors in the (x) values. Each value of Xr (r = 1, 2, 3, etc.) has a corresponding calculated y for the polynomial, and the difference between this regional and the observed value is called the residual Δr in Yr so,

$$\Delta r = (a+ bxr + cxr2 + ...)$$

The principle underlying the fitting of the polynomial to make the sum of the residual squares as small as possible by choosing appropriate values for a, b, c, etc. The sum of residual squares (E) is expressed by:

$$I = n\ 2$$

$$E = \sum \Delta$$

$$I = 1$$

The best fitting of a polynomial of a given order is found when (E) is minimized. High order polynomials may produce unwanted spikes between data points and then interpolation is necessary. Increasing the order of the polynomial can decrease the minimum value of (E) which lessens the smoothing of the data. In extreme cases the order is equal to [n-1] and the polynomial passes through each of the data points. This is called interpolating polynomial for which (E) = 0 and there is no smoothing of data (Ahmed, 1994).

The best fitting of a polynomial of a given order is found when (E) is minimized. High order polynomials may produce unwanted spikes between data points and then interpolation is necessary. Increasing the order of the polynomial can decrease the minimum

value of (E) which lessens the smoothing of the data. In extreme cases the order is equal to [n-1] and the polynomial passes through each of the data points. This is called interpolating polynomial for which [E = 0] and there is no smoothing of data (Ahmed, 1994).

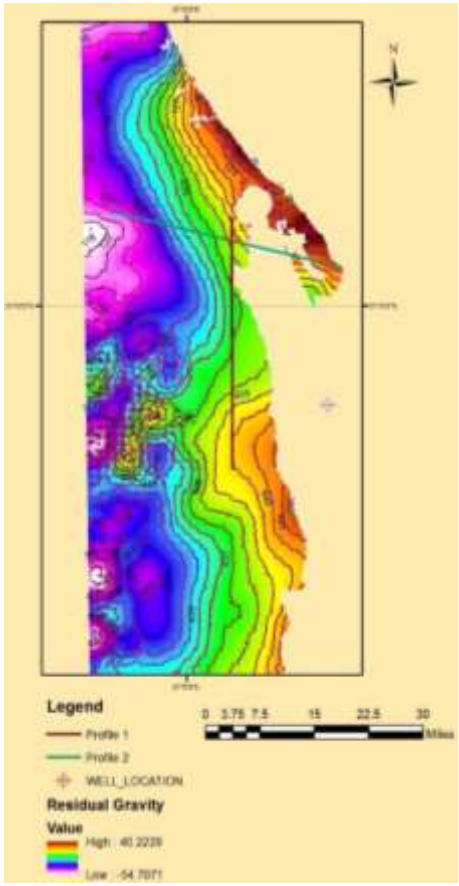

Fig (5.3.): Showing Residual Gravity map for Northern Red Sea region. Contour interval is 5mGal.

5.2.2.2. **Second Vertical Derivative**

The Second Vertical Derivative technique was used as two dimensional filters for interpretation of potential field data (Henderson & Zietz, 1949; Elkins, 1951; Darby and Davies 1967, Zurfluch, 1967; Mesko, 1965; Dobrin, 1976 and Nettleton, 1976).

This technique was developed by Elkins (1951). If we use the symbol (g) to represent gravity a choose axes so that (z) is vertical downward, then the second derivative is the quantity [d2g/dz2].

The importance of the second derivative for potential field interpretation arises from the fact that the double differentiation with respect to depth tends to emphasize the smaller, shallower geological anomalies at the expense of larger, regional feature (Elkins 1951).

The second derivative of a gravity field can be shown to be a measure of the curvature of the field. Considering a gravity profile, where the curvature of the line is greatest (radius least), the second derivative has its higher value. Where there is no curvature, (radius infinite), the second derivative is zero. If a shallow geological feature of limited lateral extent (like a salt dome) has a gravity anomaly with greater curvature than the regional field on which it is superimposed, the second derivative will be greater over the localized feature than over the part of the area where the gravity variations follows the regional trend. The second derivative accentuates shallow anomalies and suppresses deep seated effects. Points of inflections of the second derivatives, i.e. points where the second derivative value changes its sign, are geologically expressed as faults, since the gravity gradient undergoes its most rapid changes from one level to another in the vicinity of faulted areas (Ibrahim, 1993).

The main objective of Appling the derivative in the research study is for the delineation of shallow faults.

As shown in figure (5.4. A and 5.4. B) The derivative has a higher value at the greatest curvature (crest or trough) and has a zero value where there is no curvature i.e. at point of inflection; this phenomenon could geologically represented by the presence of a fault. Therefore, the importance of applying the second derivative technique in this research study is to help fault detection and delineation.

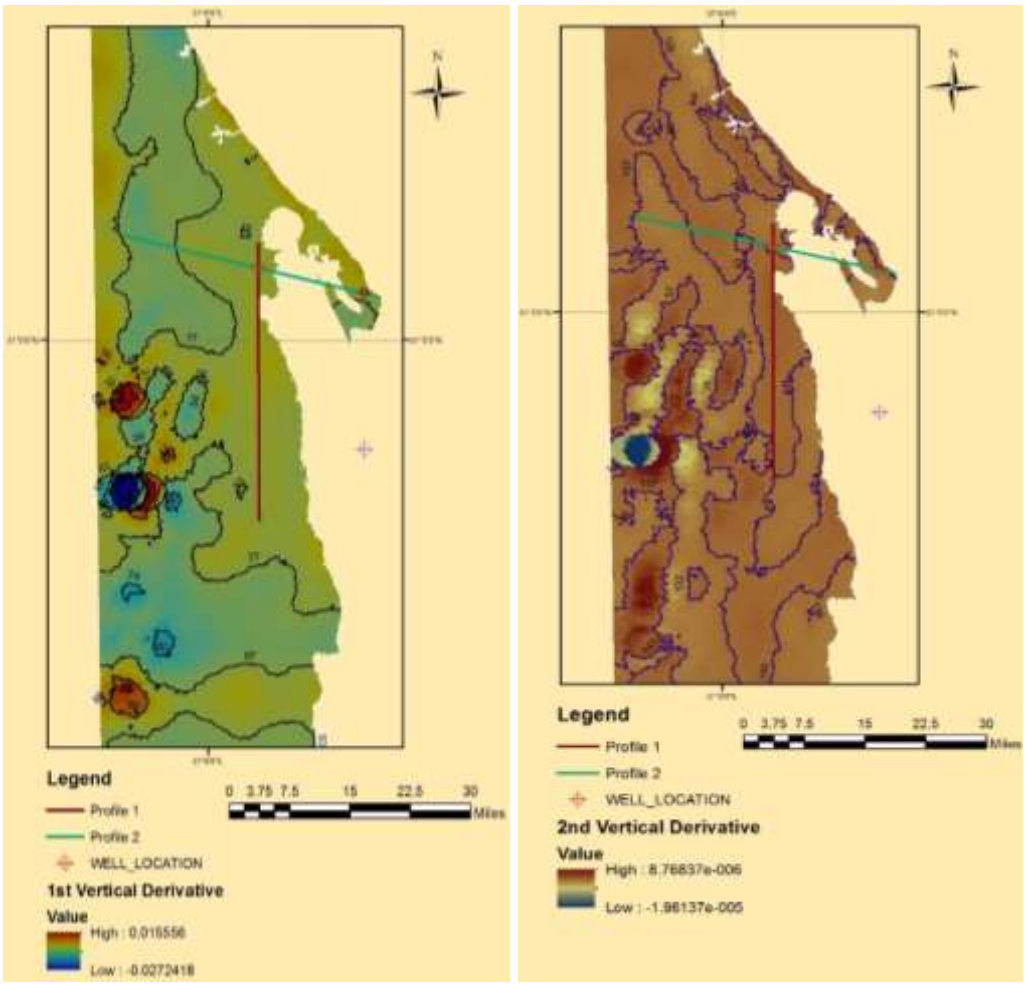

Fig (5.4. A): shows a first vertical derivative map, and **Fig (5.4. B):** second vertical derivative of the study area, on which the zero contours line separates the positive from the negative anomalies. These separated anomalies indicate varying lithological units.

Many structural trends could be distinguished from the images. The filter is found very useful in delineating normal faults with large throws associated with high gradient anomalies whereas derivative anomalies are less apparent where the gradients are much lower. In this case faults can only be suggested, and other tests of data are needed.

5.2.2.3. **First horizontal derivative**

The first horizontal derivative may be qualitatively interpreted by considering the zones of maximum gradients for determining probable fault system and/or lithological contacts, which are present in the area (Fig. 5.5). Therefore, it is possible from derivative maps to delineate the following features:

In figure (5.5) shows, contains a linear maximum gradient trending NW and NE. In the northern part of the first horizontal derivative map: there are three linear patterns of dense contours oriented in a NE and NW direction. The extension of maximum horizontal gradient zones and their orientation are utilized to determine faults extension and their orientations respectively.

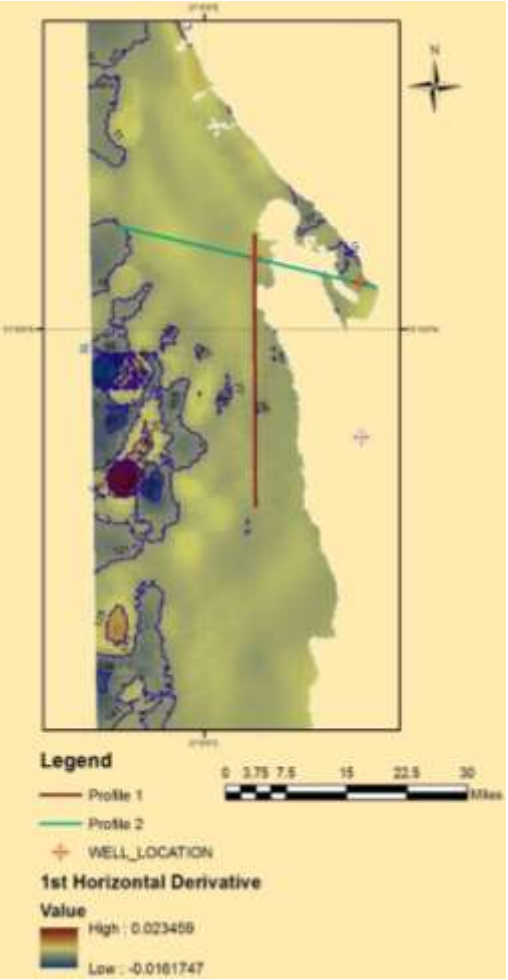

Fig (5.5.): Showing First horizontal derivative map for Northern Red Sea region.

5.2.3. **2.5D Modeling:**

Quantitative Interpretation (non-linear method) calls for approximation of the geological bodies, which are considered to be the gravity source, by assuming simple geometric model from which the theoretical gravity effect can be compared with the observed gravity data and the shape of the body can be changed (modified) to minimize the difference between the observed and the computed gravity effects, often by interactive and/or iterative computer inversion methods (Kearey and Brooks, 1988).

The modeling technique calls for approximation of the geological feature considered being the source by assigning it a simple geometrical form for which the gravity field can be computed mathematically by specified dimension and various values can be assigned to the parameters describing the geometry of these bodies. The model is not truly 3D because it is assumed to be uniform in the third dimension, it is more than 2D. Hence the term '2.5D' modeling of the anomalies. In this study was performed by Talwani program. Three profiles has been created in the study area **Profile I** are NS trending, **Profile II** are trending NW-SE and **Profile III** are trending NW-SE The profiles technique is used to examine unexplained anomalies.

5.2.4. **Density Measurements:**

The interpreter of the gravity data is interested in determining the subsurface variations of mass and this process requires that the density of the material of interest or the density contrast between the surrounding materials be known. For this reason especial attention is paid to the densities and the density contrasts between different representative rock types in the surveyed area. Robertson Research International (1988) provided density measurements for all the sedimentary formations (2.40 g/ cm3) and the Basement rocks of the area (2.73 g/ cm3). So the density contrast is (-0.33 g/cm3).

5.2.5. **Residual gravity models:**

5.2.5.1. **Profile (I)**

This profile is cutting across the eastern part of the surveyed area in proper N-S trend figure (5.6.). The residual anomaly profile delineated the structural trend which turned out to be grabin-dominated faults. This profile is passing across Dunghunab-1 well.

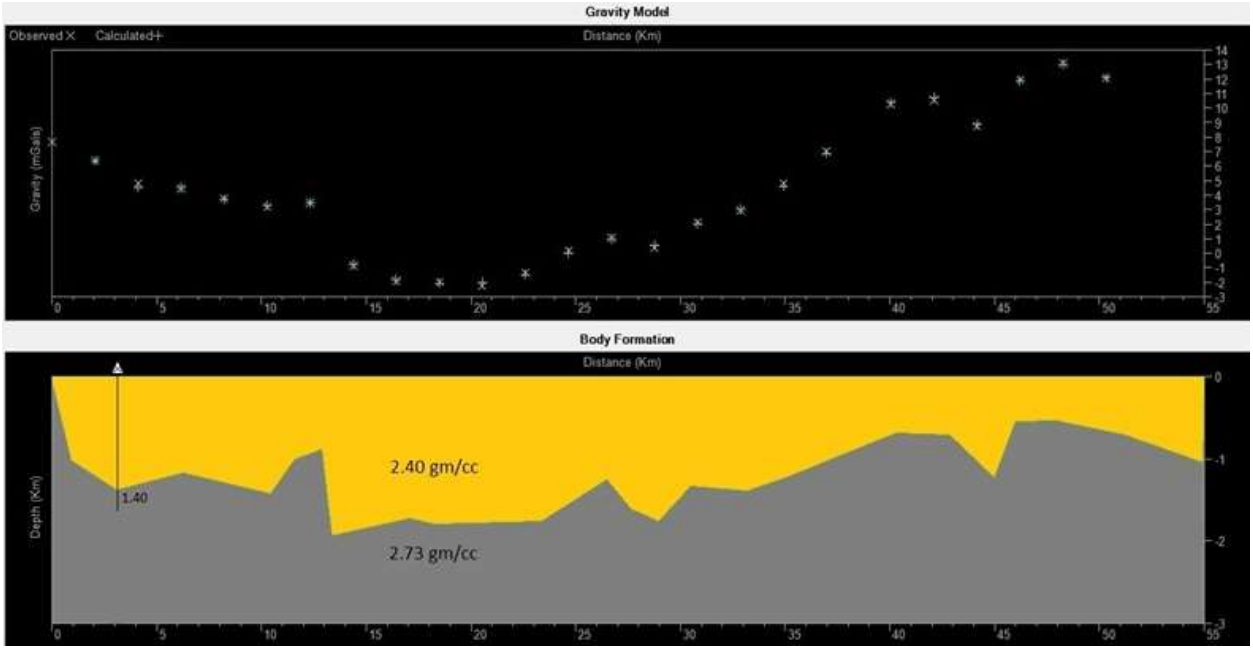

Fig (5.6.): Residual gravity model for profile (I).

5.2.5.2. **Profile (II)**

This profile is cutting across the north-east part of the study area in proper NW-SE trend figure (5.7.). The residual anomaly profile defines grabin faults bounded by normal faults. This profile is passing across Abu Shagara-1 well.

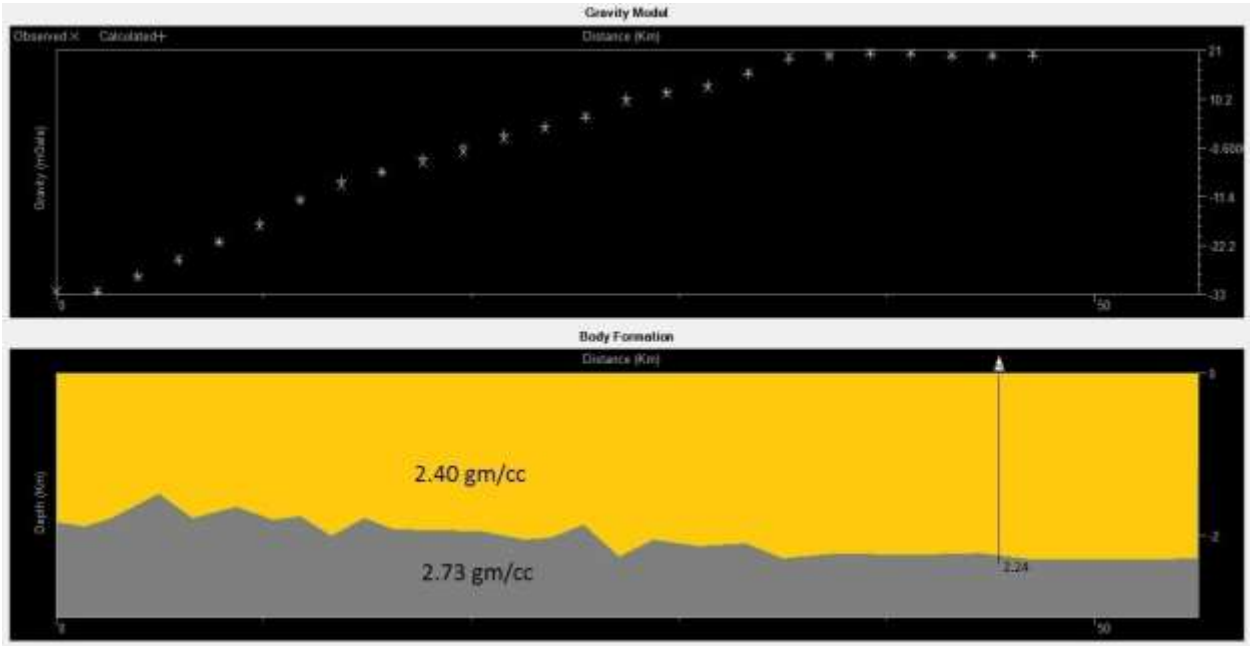

Fig (5.7.): Residual gravity model for profile (II).

5.3. **Geological section:**

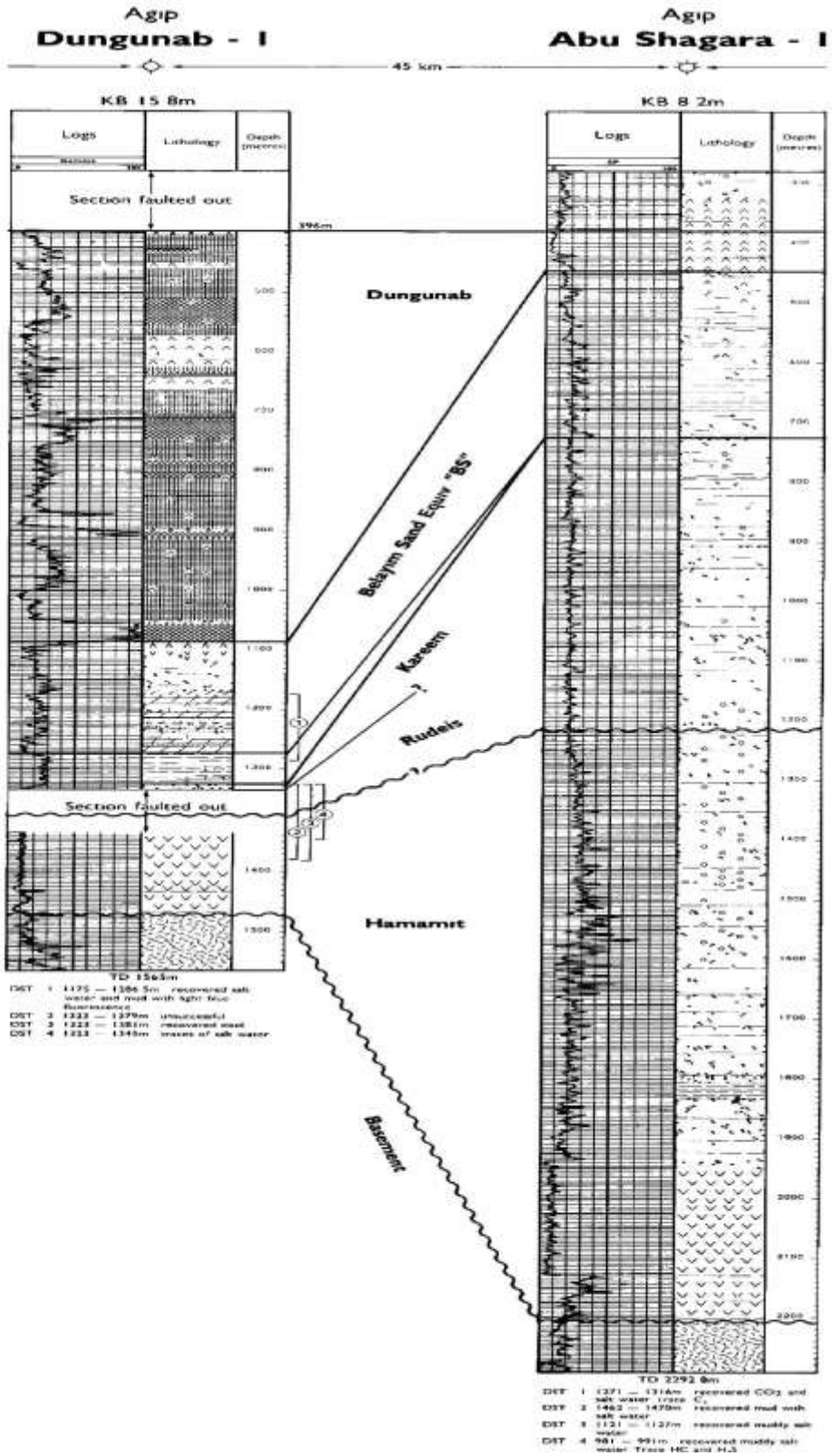

Chapter Six

Conclusion & Recommendations

Conclusions:

- The Gravity and Remote Sensing data are incorporated with surface geology to study the subsurface geology of North Port Sudan and its offshore continuation. All the images have been used simultaneously to produce the geological map of the study area in the GIS environment.
- Two residual gravity profiles are constructed cutting the most prominent anomalies in the area. For profiles 1 and 2 the residual anomaly for a presumed model constrained by the geology of the area is calculated. Sediments depth to basement is constructed from these models. In profile 1, the well intersects at 1400 m (actual depth 1470 m). In profile 2, the well intersects at 2240 m (actual depth 2210 m).
- Normal fault is the dominant fault type. Which produced combination of step faults, horst and graben structures. This intensive faulting can be attributed to the extension forces acting on the stretching crust of the area.

Recommendations:

- This approach led to accurate results, hence we recommend to adopt it in prospective studies and researches.
- We recommend to apply this method throughout the coast of the Sudanese Red Sea.
- According to our models, we recommend to drill more wells in the southern part of the study area.

References

Abu Fatima, M. (1992): Magmatic and tectonic evolution of the granite-greenstone sequences of the Sinkat area, Red Sea Province, NE Sudan. Unpubl. Mphil. Dept.Geol., Univ. of Portsmouth, UK, 276pp.

Abrams, M.J., Brown, D., Lepley, L. and Sadwski, R. (1983): Remote Sensing for porphyry copper deposits in Southern Arizona. Elpaso Texas. Econ. Geol., 78,591604.

Babiker, M and Gudmundsson, A. (2004): Geometry, structure and emplacement of mafic dykes in the Red Sea Hills, Sudan. Journal of African Earth Science, volume 38, pp 279 – 292.

Brown, G. C. (1980): Calc-alkaline magma genesis. The Pan-African contribution to crustal growth. In: Al-Shanti, A. M. S. (Ed.). Evolution and mineralization of the Arabian-Nubian Shield. IAG Bull. 3, 3, 19-29.

Bunter, M. A. G and Abel Magid, A. E. M. (1989): The Sudanese Red Sea 1, new development in stratigraphy and petroleum - geological evolution. Journal of petroleum Geology, Volume 2, pp 145 -166.

Cocharan, J. R., (1981): Simple models of diffuse extension and the pre-seafloor spreading development of the continental margin of the northern Gulf of Aden. Oceano/ogica Acta, 26th Intern. Geol. Cong. Proc., 155- 165.

Crane, R.B. (1971): Preprocessing Techniques to reduce atmospheric and sensor variability in multispectral scanner data. Proceedings of the 7th International Symposium on Remote Sensing of Environment. Ann. Arbor. Michigan. 1345 pp.

David T. Sandwell and Walter H. F. (1997): Exploring the Ocean Basins with Satellite Altimeter Data.

Drake, C. L. and Girdler, R. W., (1964): A Geophysical study of the Red Sea. Geophys. Jour. Roy. Astr. Soc., 8, 473-495.

Elkins, T .A. (1951): The second derivative method of gravity interpretation Geophysics, Vol. 16, pp.29-50.

Eklundh, L. and Singh, A. (1993): A comparative analysis of standardized and unstandardized principal components analysis. Int. J. Remote Sensing. 14(7), 1359-1370.

El Nadi, A. H. (1984): The geology of the late Precambrian metavolcanics, Red Sea Hills, northeast Sudan. Ph. D. Thesis, University of Nottingham.

El Tom, M. A. (1991): An outline of the climate of the Red Sea Region of the Sudan. RESAP technical papers, Khartoum University Press, 17 p.

Holmes, A. (1951): The sequence of Precambrian Orogenic belts in South and Central Africa. 18th Int. Geol. Congr., London, 14, 254-269.

Konstantinov, N, Babikir, H. M, El Tahir, A. M and Medani, A. H. (1973): The gypsum deposits of the Bir Eit area (unpublished report), geological surveying and mineral exploration project, Red Sea Hills.

Musab A. Eljah, Esamaldeen Ali, Abdalla E. M. Elsheikh, Khalid A. Elsayed Zeinelabdein (2015): Geological and Tectonic Setting of the Kamoreib Metavolcanics, Southern Hamisana Area, Red Sea Hills, NE Sudan. Faculty of Petroleum and Minerals, American Journal of Earth Sciences. Vol. 2, pp. 43-51.

Qureshi (1971): Gravity Measurements in the North-eastern Sudan

Robert J. Stern, Peter R. Johnson, Alfred Kröner and Bisrat Yibas: Neoproterozoic Ophiolites of the Arabian-Nubian Shield.

Robertson Research (R.R.I). (1984): Robertson Research International Limited, United Kingdom.

Robertson Research (R.R.I). (1985): An evolution of the Suakin discovery in the Red Sea, and discussion on the exploration potential of the area. Robertson Research international Limited, United Kingdom, 22 p.

Sabins, F. Floyd (1997): Remote-Sensing Principles & Interpretation. 3rd ed. Freeman & Co, New York, USA.

Sabins, F. Floyd (1999): Remote Sensing for Mineral Exploration. Ore Geol. Rev., 14. Elsevier Science.

Sestini (1965): Cenozoic Stratigraphy and Depositional History,
Red sea coast, Sudan. Bulletin of the American Association of Petroleum Geologists vol. 49, no. 9 (September. 1965). Pp. 1453-1472.

Talwani, M., Worzel, J. L. and Landisman, M., (1959): Rapid gravity computation for two-dimensional bodies with application to the Mendocino fracture zone. J. Geophys. Res. 46, 49-59.